and glial cells in patients with sporadic ALS and FTLD with ubiquitin-positive inclusions (FTLD-U) [3, 34]. Subsequently, missense mutations in the TDP-43 gene (*TARDBP*) were found to be a genetic cause of a familial form of ALS (FALS), ALS10 [15, 20, 38, 40, 43], indicating that an abnormality in TDP-43 causes the disease. TDP-43 belongs to a member of the heterogeneous nuclear ribonucleoprotein family and is involved in multiple steps of gene expression, such as transcriptional regulation, pre-mRNA splicing and translational regulation [42]. In the normal brain, TDP-43 resides predominantly in the nucleus, whereas pathological TDP-43 accumulation occurs mostly in the cytoplasm or neuronal processes [3, 34].

Mutation analyses for genes having a similar structure with TDP-43 then led to the identification of mutations in the gene encoding another RNA-binding protein, FUS, in cases with FALS type 6 (ALS6) [21, 41]. ALS6 is characterized neuropathologically by the occurrence of neuronal cytoplasmic inclusions (NCIs) that have been called basophilic inclusion bodies. The NCIs in ALS6 are immunostained positively for FUS. FUS-positive NCIs have been identified in some forms of tau and TDP-43 negative FTLD. Such diseases include atypical FTLD-U, basophilic inclusion body disease and neuronal intermediate filament inclusion disease. FUS is a 526 amino acid, multi-functional protein that is involved in many aspects of gene expression [35, 44].

Now, FTLD with TDP-43- and FUS-positive inclusions are assigned as FTLD-TDP and FTLD-FUS, respectively. Subpopulations of both FTLD-TDP and FTLD-FUS are associated with ALS pathology, while mutations in TDP-43 and FUS genes cause FALS with NCIs that contain the mutated gene products. Similarities in the functions, molecular structures and subcellular localizations of FUS and TDP-43 also suggest that the pathophysiologies of these diseases are related. Like TDP-43, FUS-immunoreactivity is considered to be localized normally to the nucleus in postmortem human brain tissues, but pathological FUS accumulation occurs in the neuronal cytoplasm [5, 26, 30, 32, 33, 41]. FALS-linked *FUS* mutations that affect the nuclear localization signals (NLS) are known to cause assembly of FUS into stress granules, a type of cytoplasmic RNA–protein complexes [8, 11]. Thus, similarly to FTLD-TDP, translocation of FUS from the nucleus to the cytoplasm may play an essential role in the formation of pathological cytoplasmic aggregates in FTLD-FUS.

There is literature that describes localization of FUS to dendritic spines in primary cultured mouse hippocampal neurons [12]. Immunohistochemistry of normal mouse hippocampal tissues also demonstrated its localization to the dendrites [6]. Studies on postmortem human brain tissue indicated that, based on the amount of normal physiological staining by immunohistochemistry, the anti-FUS sensitivity was greatly influenced by the degree of tissue fixation [26, 30, 32, 33]. In the present study, therefore, we used lightly fixed, free-floating sections of postmortem human brains. We report here that, in humans, FUS is present not only in the nucleus and cell bodies but also in neuronal processes under physiological conditions. Our results demonstrate FUS-positive granular staining in the neuropil in postmortem human brain tissues. The granular staining is associated with synapses and is often located along with microtubule-associated protein 2 (MAP2)-positive dendrites. While dendritic FUS-immunoreactivity occurs constitutively in some brain regions, it is increased in the cortex of FTLD-TDP and, less markedly, in Alzheimer's disease (AD).

Materials and methods

Cases

We examined 24 cases: 9 normal subjects, 9 patients with AD, 5 with FTLD-TDP, and a patient with FTLD-FUS (for age, sex, and postmortem delay, see supplementary Table 1). No case had any family history of neurological or psychiatric disorder. Neuropathological diagnoses of AD, FTLD-TDP and FTLD-FUS were made in accordance with published guidelines [1, 10, 28, 29]. In FTLD-TDP, the TDP-43 pathology type was type A in a case and type C in the other four cases [27]. The FTLD-FUS subtype was neuronal intermediate filament inclusion disease [29]. All AD cases were studied in a previous study [4], in which they were shown to lack simultaneous TDP-43 accumulation in the amygdala, hippocampus, entorhinal cortex and temporal neocortex. For autopsied human materials, consent was obtained for every autopsy for pathological assessment and research use. This study was approved by Tokyo Metropolitan Institute of Medical Science (TMIMS) Research Ethics Committee.

Immunohistochemical staining

Small blocks of brain tissues were dissected at autopsy and fixed in 4 % paraformaldehyde (PFA) in 0.1 M phosphate buffer (pH 7.4) for 2 days in the cold. Brain regions sampled for qualitative assessment of FUS in control brain included the frontal cortex, insular cortex, hippocampus and adjacent parahippocampal gyrus, striatum, cerebellar cortex, midbrain, pons, medulla oblongata and the spinal cord. For quantitative analyses of neuropil FUS granules in control, AD and FTLD cases, hippocampal tissues containing the parahippocampal neocortex were employed. Following cryoprotection in 15 % sucrose in 0.01 M phosphate-buffered physiological saline (PBS, pH 7.4),

brain blocks were cut on a freezing microtome into free-floating sections of 30 μm thickness. For immunohistochemical staining, the sections were first incubated with 0.5 % H_2O_2 in PBS for 30 min. Sections were blocked with 10 % normal goat or bovine serum in PBS containing 0.3 % Triton X-100 (Tx-PBS), and then incubated overnight at 4 °C with the primary antibodies at the appropriate dilution. Antibodies employed in this study are summarized in Table 1. Following incubation with the appropriate secondary antibody, labeling was detected using the avidin-biotinylated HRP complex (ABC) system (Vector Laboratories, Burlingame, CA) coupled with a 3,3,-diaminobenzidine tetrachloride reaction to yield a brown precipitate.

Mice were terminally anesthetized and perfused with PBS and then 4 % PFA. Brains were removed and treated for immunohistochemistry, similarly to the human tissue sections. The mouse experiment was done in accordance with the guidelines of TMIMS and with the permission of the TMIMS's ethical committee for animal experiments.

For double labeling immunofluorescence analyses, sections were incubated overnight at 4 °C with the antibodies to FUS (HPA-008784) and MAP2, phosphorylated neurofilament or synaptophysin. These were employed as a dendritic marker, axonal marker and synaptic marker, respectively. Sections were then incubated in a cocktail of fluorescein isothiocyanate (FITC)-conjugated goat anti-mouse IgG (1:100, Millipore, Temecula, CA) and tetramethylrhodamine isothiocyanate (TRITC)-conjugated goat anti-rabbit IgG (1:100, Millipore). After incubation in 0.1 % Sudan Black, sections were observed by a confocal laser microscope (LSM5 PASCAL; Carl Zeiss MicroImaging GmbH, Jena, Germany).

Table 1 Antibodies

Antibody to	Type	Source	Dilution
FUS [1–50] (A300-302A)	Rabbit	Bethyl[b]	1:1,000 1:3,000 (WB)
FUS [1–50] (ab84078)	Rabbit	Abcam[c]	1:1,000 1:3,000 (WB)
FUS [86–213] (HPA-008784)	Rabbit	Sigma[d]	1:2,000 1:500 (IF) 1:3,000 (WB)
FUS [52–400] (11570-1-AP)	Rabbit	Prot.[e]	1:1,000 1:3,000 (WB)
FUS [400–450] (A300-293A)	Rabbit	Bethyl	1:1,000 1:3,000 (WB)
FUS [C-term] (sc-47711)	Mouse	S.C.[f]	1:200 1:500 (WB)
Microtubule-associated protein (MAP)-2	Mouse	Sigma	1:500 (IF)
Phosphorylated neurofilament[a]	Mouse	Stb[g]	1:500 (IF)
Synaptophysin (clone SY38)	Mouse	Dako[h]	1:1,000 1:500 (IF) 1:6,000 (WB)
PSD95	Mouse	Millipore[i]	1:2,000 (WB)
β-Actin	Mouse	Sigma	1:5,000 (WB)
α-Tubulin	Mouse	Sigma	1:5,000 (WB)

IF immunofluorescence, *WB* western blotting, *rabbit* rabbit polyclonal, *mouse* mouse monoclonal

[a] SMI31; [b] Bethyl, Montgomery, TX; [c] Abcam, Cambridge, UK; [d] Sigma-Aldrich, St. Louis, MO; [e] Proteintech, Chicago, IL; [f] Santacruz, Santacruz, CA; [g] Sternberger I, Bethesda, MA; [h] Dako, Glostrup, Denmark; [i] Millipore, Billerica, MA

Western blot

Fresh frozen tissue of the inferior temporal cortex from a normal subject was employed for western blot (65 years, female). To analyze the tissue distribution of FUS in the whole body, the brain, lung, liver, spleen, pancreas, kidney, heart, muscle, testes, and thymus of adult male C57BL/6J mice were used. Each tissue sample was homogenized by sonication in the lysis buffer [10 mM Tris–HCl pH 7.4, 150 mM NaCl, 5 mM EDTA, 1 % Triton, 1 % sodium dodecyl sulfate (SDS), 0.5 % sodium deoxycholate and complete protease inhibitor cocktail (Roche)]. After centrifugation at 20,000*g* for 30 min, the supernatants were collected for western blot analysis. Total protein in the lysates was quantified using the Pierce BCA Protein Assay kit (Rockford, IL, USA) with bovine serum albumin (BSA) as a standard. Western blot analysis was performed as described previously [18]. The primary antibodies were used at the appropriate dilutions as shown in Table 1.

Subcellular fractionation

The synaptosomal fraction was obtained as previously reported [17]. Further subcellular fractionation was carried out as previously described with slight modifications [9, 16]. In brief, the synaptosomal fraction was suspended in 10 volumes of ice-cold 0.1 mM $CaCl_2$. An equal volume of 2 % Triton X-100 in 40 mM Tris HCl buffer, pH 6.0, was added to incubate the sample in the solubilization buffer (1 % Triton X-100 in 20 mM Tris HCl buffer, pH 6.0) on ice for 30 min with gentle inverting. The sample was then centrifuged at 40,000*g* for 30 min. The supernatant was collected and assigned as the synaptic vesicles (SVs) fraction. The pellet was re-suspended in pH 8.0 solubilization buffer and incubated on ice for 30 min with gentle inverting. After centrifugation at 40,000*g* for 30 min, the supernatant was collected and assigned as the pre-synaptic fraction. The remaining pellet was solubilized in 5 % SDS and assigned as the post-synaptic density (PSD) fraction. The SVs and pre-synaptic fractions were combined and precipitated with chilled acetone and spun down at 20,000*g*. The precipitated protein was solubilized in 5 % SDS. Total protein was quantified using the Pierce BCA Protein Assay kit (Rockforop, IL, USA) on every sample.

Morphometric analyses

For tissue quantification, a set of sections of the parahippocampal neocortex from all cases were immunostained under identical conditions with anti-FUS antibody (HPA-008784) and counterstained with haematoxylin and the other set were stained with anti-synaptophysin. An observer (N.A.) who was blinded for the patient ID and clinical data performed both image acquisition and subsequent digital image analysis. For each case, 3 digital images (2,000 × 2,000 pixels) were captured randomly from layer II with a 40× objective and Olympus digital CCD camera (DP71). All nuclear areas stained for haematoxylin were dissected out manually, using Photoshop CS5 (Adobe Systems, Tokyo), regardless of the staining intensity for FUS. Then the number of immunopositive pixels was counted using the ImageJ/NIH Image software (http://rsbweb.nih.gov/ij/). The same threshold value was applied to all sections. The pixel counts obtained from FUS staining were divided by those from synaptophysin staining in every case. Statistical analyses were performed by Mann–Whitney *U* tests on a statistics software, GraphPad Prism version 5.0® (GraphPad Software, San Diego, CA, USA).

Results

Immunochemical characterization of FUS protein in the brain

To characterize immunochemically the FUS protein in human and mouse brains, we carried out western blot analyses using six commercially available antibodies that

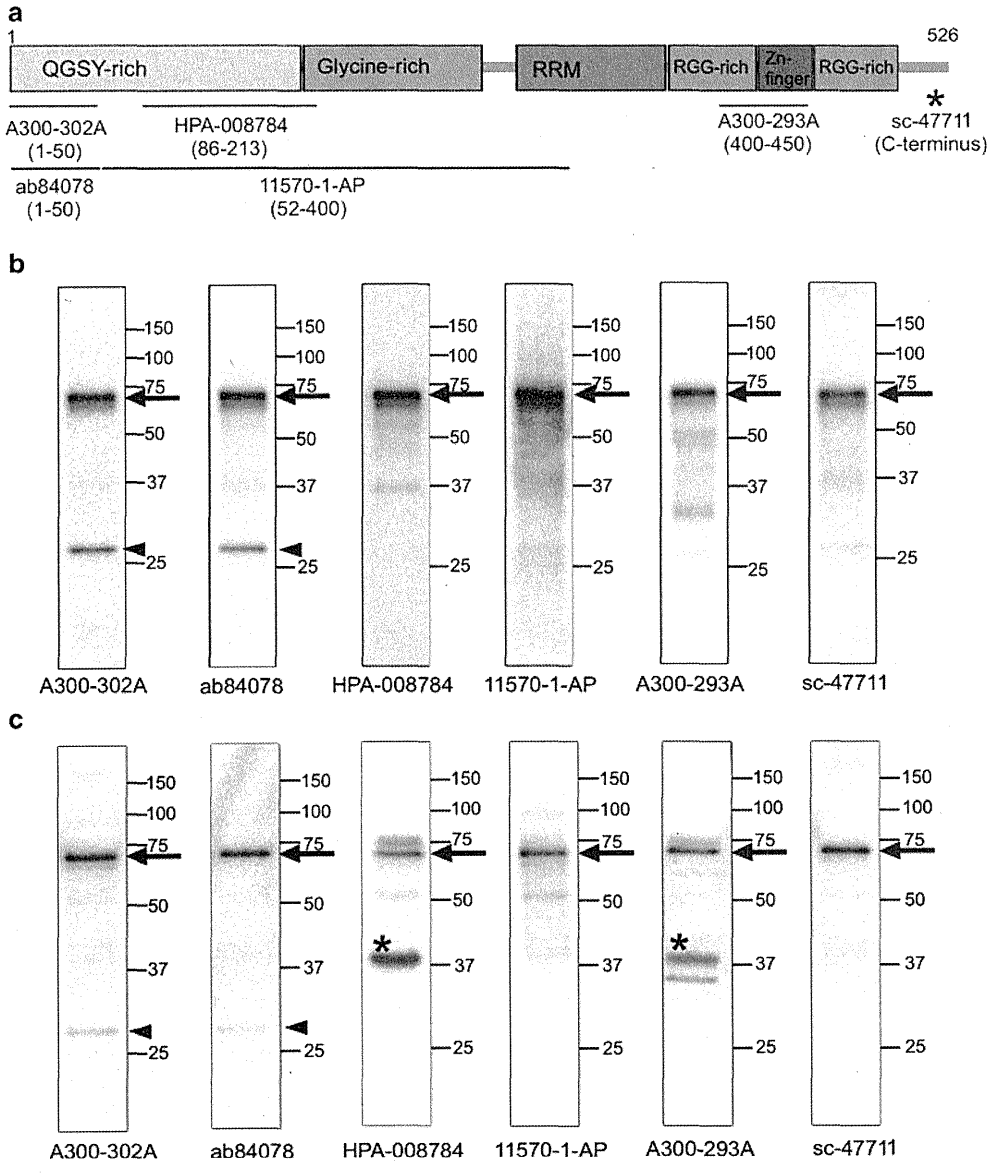

Fig. 1 Characterization of six commercially available antibodies to FUS (A300-302A, ab84078, HPA-008784, 11570-1-AP, A300-293A and sc-47711). **a** Portions of the FUS molecule used for generation of these antibodies are shown in the domain architecture of human FUS. Information was obtained from the data sheets published by each company. *Asterisk* The portion for generation of sc-47711 was not available, except for it being the carboxy-terminus. **b** and **c** Western blot with the six antibodies of an inferior temporal cortex sample from a control subject (**b**) and the whole brain of adult C57BL/6J mice (**c**). In both human and mouse, all antibodies detect a major band migrating at approximately 72 kDa (*arrows*), which corresponds to full-length FUS. Two additional minor bands at 28 kDa (*arrowheads*) and 37 kDa (*asterisks*), respectively, are also recognized by some but not all antibodies

recognize different regions of the FUS molecule (Fig. 1a). All antibodies detected a major band of 72 kDa that corresponds to full-length FUS in human brain extracts. An extra minor band of 28 kDa was detected by two anti-FUS antibodies, A300-302A and ab84078, which were raised against the N-terminal regions. We also analyzed mouse whole brain extracts. All six anti-human FUS antibodies recognized the 72 kDa major band. The two anti-N-terminal region antibodies again revealed the 28 kDa minor band. Two other antibodies, HPA-008784 and A300-293A, detected an additional minor band at approximately 37 kDa. This band was not seen in human brain extracts or in the mouse blot with anti-FUS (52-400), 11570-1-AP. The 37 kDa band, together with the 72 kDa major band, disappeared in a competition study for A300-293A with antigen peptide (Bethyl, Montgomery, TX) and by replacement of the primary antibody with non-immunized rabbit immunoglobulin (data not shown). Thus, further studies are required to clarify whether the 37 kDa band is derived from a cross-reaction to an indifferent molecule or a mouse-specific FUS fragment.

We then investigated the distribution of FUS in mouse tissues by western blot analyses (Fig. 2). FUS was expressed ubiquitously but most abundantly in the brain, lung, spleen, testis and thymus. Less, but significant expression was seen in the liver, heart and muscle and, to a lesser extent, in the pancreas and kidney. In all organs investigated, FUS was predominantly a 72 kDa protein.

Localization of FUS in control human brain

We then investigated the immunohistochemical localization of FUS in control human brains. We applied the six different anti-FUS antibodies to lightly fixed, frozen-cut free-floating sections. Consistent with previous reports [32, 33], all anti-FUS antibodies revealed predominant FUS localization to the nucleus in the cerebral cortices, together with occasional, faint cytoplasmic staining (Fig. 3a, b; Supplementary Fig. 1a, b). In addition, FUS was detected in the form of small granular structures in the neuropil of the substantia nigra pars compacta (SNpc). Of the six antibodies employed, those raised against the middle portion of FUS, HPA-008784 and 11570-1-AP, labeled the neuropil granules more intensely than the other antibodies (Fig. 3c, d; Supplementary Fig. 1c, d). We therefore employed HPA-008784 to investigate further the distribution of FUS-positive neuropil granules in various brain regions.

Figure 4a–c illustrates FUS-immunoreactivity in the cerebral cortices. In the neocortex, nuclear staining predominated over the sparsely found neuropil granules (Fig. 4a). The neuropil granules were relatively frequent in the supragranular layers compared with the deep cortical layers. In the subcortical white matter, the majority of glial nuclei were negative for FUS (data not shown). In the pyramidal layer of the hippocampal cornu ammonis (CA) regions (Fig. 4b) and the subiculum, the nuclear staining was less intense than in the neocortex, but the neuropil granules were more frequent. In the dentate granular cell layer, FUS was almost exclusively localized to the nuclei (Fig. 4c). The distribution of FUS in the parahippocampal

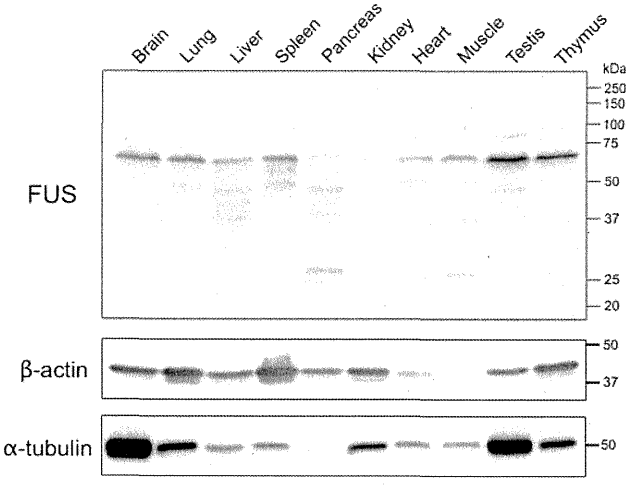

Fig. 2 Western blot of various organs of mouse with anti-FUS (11570-1-AP), anti-β-actin and anti-α-tubulin antibodies

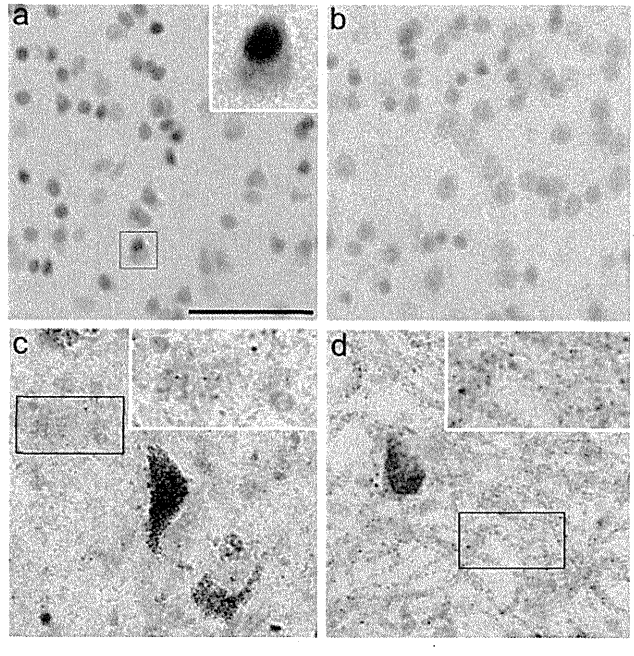

Fig. 3 FUS immunostaining of the frontal cortex (**a, b**) and the substantia nigra pars compacta (SNpc) (**c, d**) from a control subject. Antibodies used are A300-302A (**a, c**), and 11570-1-AP (**b, d**). With all antibodies, nuclear staining predominates in the frontal cortex, while neuropil granules are abundant in the SNpc. *Insets* in **a**, **c** and **d** show higher power magnification of the *boxed area*. **a–d** are at the same magnification. *Scale bar* 50 μm in **a**

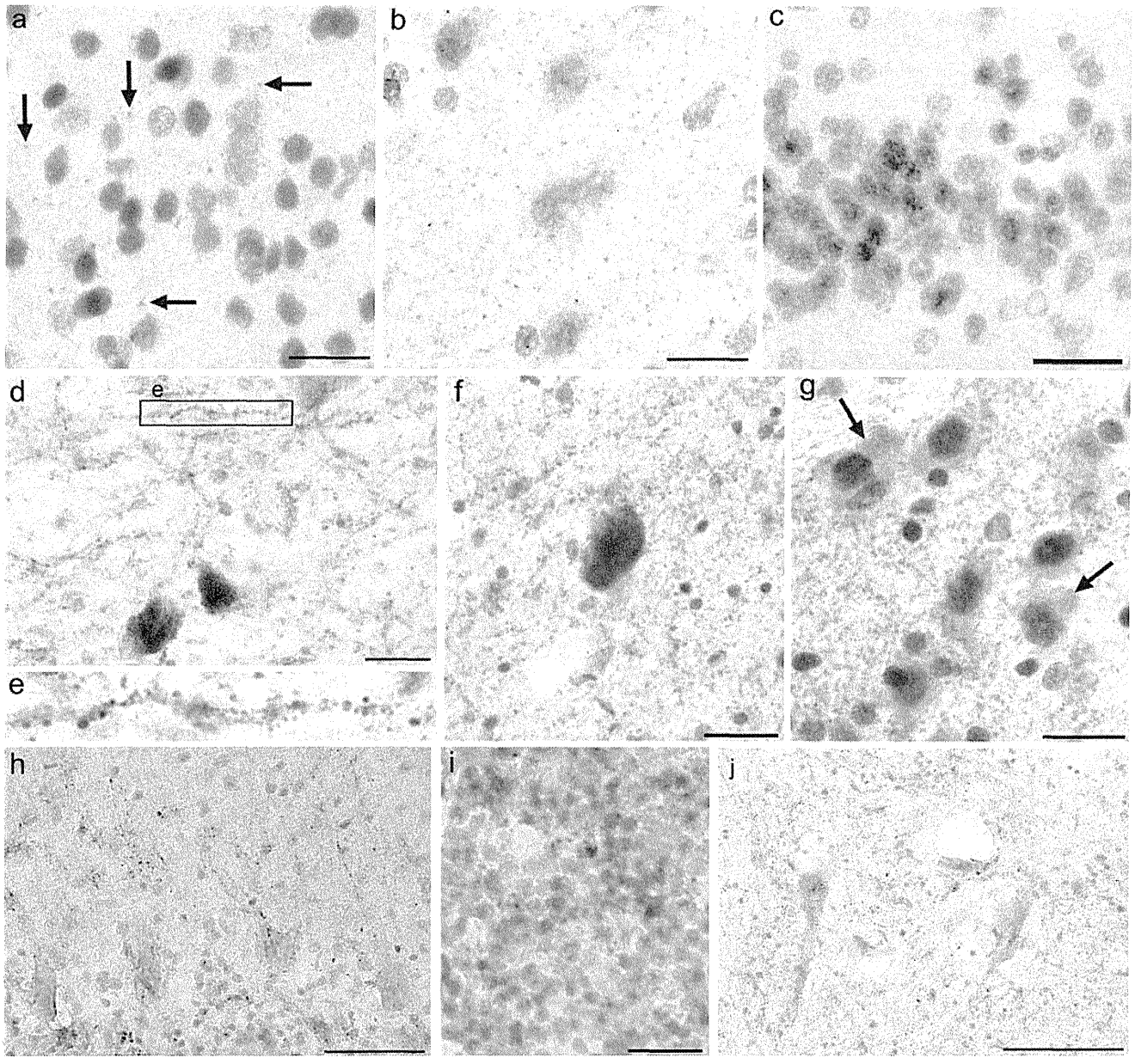

Fig. 4 Immunohistochemical staining of the control brain for FUS (HPA-008784). Layer II of the frontal cortex (**a**), the pyramidal layer of the hippocampal CA1 (**b**) and the granular layer of the dentate gyrus (**c**). *Arrows* in **a** indicate FUS-positive neuropil granules. The granular staining is more frequent in the hippocampal CA1 (**b**) and subiculum than in the neocortex (**a**) and the granular layer of the dentate gyrus (**c**). FUS-positive granules are more frequent in the brain stem: the substantia nigra pars compacta (SNpc) (**d, e**); the locus coeruleus (**f**) the pontine nucleus (**g**). The higher power photomicrograph of the *boxed area* in **d** is shown in **e**. *Arrows* in **g** indicate weak staining of neuronal cytoplasm in the pontine nucleus. In the cerebellar cortex, FUS-positive granules appear to marginate the cell body and processes of Purkinje cells (**h**). In the granular cell layer of the cerebellum, FUS-positive granules are seen with occasional FUS-positive nuclei (**i**). FUS-positive granules are also frequent in the gray matter of the spinal cord (**j**). *Scale bars* are 20 μm in **a, b, g** and **i**, 30 μm in **c, d, f** and **h**, and 100 μm in **j**

neocortex was similar to that in other areas of the cerebral neocortex.

In the caudate nucleus and putamen, FUS-positive neuropil granules were sparse (data not shown). In the SNpc, FUS-positive neuropil granules were abundant, as mentioned above (Fig. 4d). At high power magnifications, the FUS-positive neuropil granules appeared to form neuronal process-like structures (Fig. 4e). They were also abundant in the red nucleus and the locus coeruleus (Fig. 4f). In many of these brainstem areas, the majority of neuronal nuclei and cytoplasm were either negative or only faintly positive for FUS. In the pontine nucleus (Fig. 4g), FUS was localized to both the nucleus and neuropil granules. In the medulla oblongata, granular staining

predominated over the nuclear staining in the inferior olivary nucleus, while both nuclear and granular staining were evident in the hypoglossal nucleus. Weak staining was seen in the neuronal cytoplasm in the pontine nucleus and the hypoglossal nucleus. In the cerebellar Purkinje cell layer, granular FUS-immunoreactivity appeared to be located around the cell bodies and processes of Purkinje cells, the latter of which extended towards the outer molecular layer (Fig. 4h). Nuclear and cytoplasmic staining was either absent or very weak. Whether or not the FUS-positive granules were present within the cytoplasm was not determined with certainty in the 30 μm thick sections. In the cerebellar granular cell layer, only a small portion of the nuclei were positive for FUS, while granular FUS-immunoreactivity was frequent (Fig. 4i). In the spinal cord, granular FUS-immunoreactivity was abundant in the gray matter (Fig. 4j). They appeared to line along with the neuronal processes, a finding which was similar to that in the SNpc. The anterior horn cells showed diffuse nuclear and cytoplasmic staining and were overlaid by granular staining.

We then performed a semi-quantitative evaluation of FUS-immunoreactivity in the nucleus and neuropil granules in various brain regions (Table 2). FUS was mainly localized to the nucleus in the cerebral neocortices and the limbic areas. In the brainstem, cerebellum and spinal cord, on the other hand, FUS-positive neuropil granules were frequent. In such brain regions as the SNpc, Purkinje cell layer and spinal cord gray matter, FUS-positive neuropil granules were clearly observed, along with neuronal processes.

Table 2 Qualitative assessment of nuclear and neuropil FUS-immunoreactivity in multiple brain regions of control human brain

Brain region	Nuclear staining	Granular staining in the neuropil
Cerebrum		
Frontal cortex	+++	+
Insular cortex	+++	+
Hippocampal CA1	++	++
Dentate granular cell layer	+++	+
Subiculum	++	++
Parahippocampal neocortex	+++	+
Caudate nucleus	+++	+
Putamen	+++	+
Cerebellum		
Purkinje cell layer	+	+++
Granular cell layer	++	++
Mid brain		
Substantia nigra	+	+++
Red nucleus	+	+++
Pons		
Locus coeruleus	+	+++
Pontine nucleus	+++	+++
Medulla oblongata		
Hypoglossal Nucleus	+++	+++
Inferior olivary nucleus	+++	+++
Spinal cord		
Anterior horn	+++	+++

Granular staining in the neuropil: + rare, ++ frequent, but not spreading over the entire microscopic field; +++ very frequent, spreading over the entire microscopic field or neuronal processes can be identified as lining granules. Nuclear staining: + up to a quarter of the nuclei are positive, ++ a quarter to a half of the nuclei are positive, +++ more than half of the nuclei are positive

Localization of FUS in mouse brains

We next examined the distribution of FUS in the mouse brain, using two FUS antibodies (HPA-008784 and 11570-1-AP). While the instruction sheet of the antibody indicated application for mouse tissue only in the latter, both obtained positive staining for neuropil granules. In the cerebral cortex, hippocampus and striatum, FUS was localized predominantly to the nucleus. Neuropil granular staining was seen but relatively rare in those areas. This contrasted with the brainstem where FUS was present in both the nucleus and neuropil granules (Fig. 5), a finding which was consistent with the results in human brain. The distribution pattern of FUS in the nucleus and neuropil appears to be conserved throughout mammalian species.

Double immunofluorescence staining

To identify the subcellular localization of FUS-positive neuropil granules, we examined tissue sections of the SNpc and pontine nucleus from control brains by double immunofluorescence staining. In the SNpc, FUS-positive granules were present along with MAP-2-positive dendrites (Fig. 6a), but not with phosphorylated neurofilament (SMI-31)-positive axons (Fig. 6b). FUS-positive granules in the SNpc (Fig. 6c, arrows) and the pontine nucleus (Fig. 6d) were closely localized to the synaptophysin, a synaptic vesicle marker. At the light microscopic level, the association appeared to be a partial overlap (Fig. 6d: d1 and d2). FUS-positive neuropil granules seemed to be localized to synapses and dendrites.

Subcellular fractionation assay

We then performed a subcellular fractionation assay of mouse whole brain to identify the precise localization of

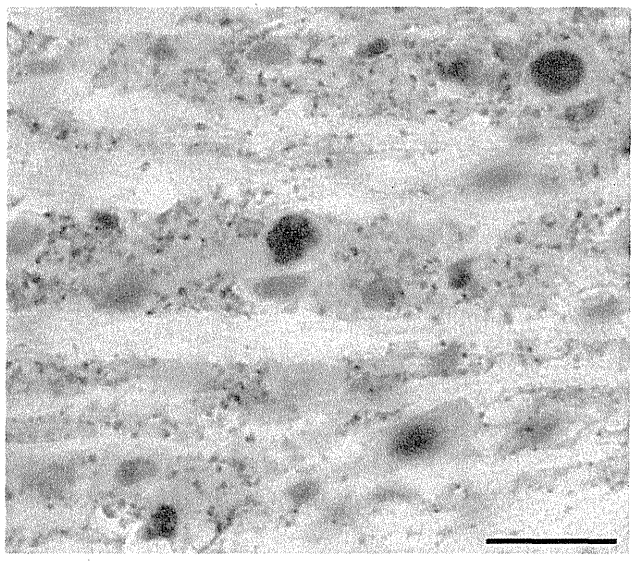

Fig. 5 Immunohistochemical staining of the mouse brain for FUS (HPA-008784). Both nuclear and granular staining is seen in the pontine nucleus. *Scale bar* 20 μm

FUS in the synapse formation. The post-synaptic density (PSD) fraction was separated from synaptic vesicles (SVs) and the pre-synaptic fraction by incubation of the synaptosomal fraction in 1 % Triton X-100 buffer and subsequent centrifugation [9, 16]. We used PSD95 and synaptophysin as markers for isolated PSD and SVs/pre-synaptic fraction, respectively (Fig. 6e). The majority of FUS in the synaptosomal fraction was sedimented to the PSD fraction and only a small amount in the SVs/pre-synaptic fraction (Fig. 6e).

FUS-positive neuropil granules increase in FTLD-TDP and AD

In addition to control subjects, we studied the hippocampus and adjacent parahippocampal neocortex of patients with FTLD-TDP and AD as well as of a patient with FTLD-FUS. FUS was not associated with senile plaques, neurofibrillary tangles or TDP-43-positive inclusions. However, FUS-positive granules appeared to be more frequent in the diseased brains than in controls (Fig. 7a, b). Tissue quantification of FUS-positive granules in layer II of the parahippocampal neocortex by computerized morphometrical analysis indicated that, following exclusion of nuclear FUS staining (Fig. 7a, b, inset), FUS-positive areas are significantly increased in FTLD-TDP ($p = 0.0010$) and AD ($p = 0.0142$) compared with control. Then the number of FUS-positive pixels was divided by that of synaptophysin-positive pixels to obtain estimate of changes in neuropil FUS granules relative to synapse density. The ratios of FUS/synaptophysin are also increased significantly in FTLD-TDP ($p = 0.0010$) and AD ($p = 0.0028$) compared with the control (Fig. 7c). These results suggest that post-synaptic FUS-positive granules are increased in some neurodegenerative conditions and that the increase is more marked in FTLD-TDP than AD. The one FTLD-FUS case showed even more FUS pixel count and higher FUS/synaptophysin ratio than any other cases (Fig. 7b, c).

Discussion

In the present study, we examined the subcellular localization of FUS in human and mouse brains. Previous immunohistochemical studies of formalin-fixed, paraffin-embedded postmortem human brain tissues for FUS showed nuclear staining in neurons and, less consistently, in glial cells, with weak labeling of neuronal cytoplasm [30, 32, 33]. Andersson et al. [2] investigated the subcellular distribution of FUS in human tissues and indicated that FUS was localized to both the cytoplasm and nucleus in most organs, but mainly to the nucleus in the brain. Other investigators, however, reported localization of FUS to dendrites and synapses in mouse hippocampal tissues and primary cultured hippocampal neurons [6, 12]. Using lightly fixed free-floating sections, we have shown that, in addition to the nucleus, a significant amount of FUS is also present as neuropil granules. By double immunofluorescence study, the neuropil FUS granules are co-localized, though often partially, with synaptophysin along with MAP-2-positive dendrites. The spatial resolution of double immunofluorescence microscopy does not permit any distinction between pre- and post-synapses [19]. The subcellular fractionation analysis of mouse brain revealed that FUS is present predominantly in the PSD fraction, indicating that the majority of the FUS-positive neuropil granules are localized to the post-synapses.

The dendritic FUS-positive granules are abundant in the brainstem and spinal cord gray matter. In control brains, they are present but not frequent in the cerebral cortex, including the hippocampus. The distribution of dendritic FUS varies significantly among brain regions, but the distribution pattern is consistent between human and mouse. The localization of dendritic FUS may be regulated by certain specific neuronal functions. Previous studies demonstrated that FUS-null primary cultured mouse hippocampal neurons exhibit abnormal spinal morphology and lower spine density [12]. It has also been reported that FUS binds to mRNAs encoding actin-related proteins, such as actin-stabilizing protein Nd1-L [13], a finding that suggests a role for the transport of mRNA to the dendrites. Together with our results, this suggests that FUS may be involved in synaptic plasticity and may regulate local translations in the dendritic spine [12, 24].

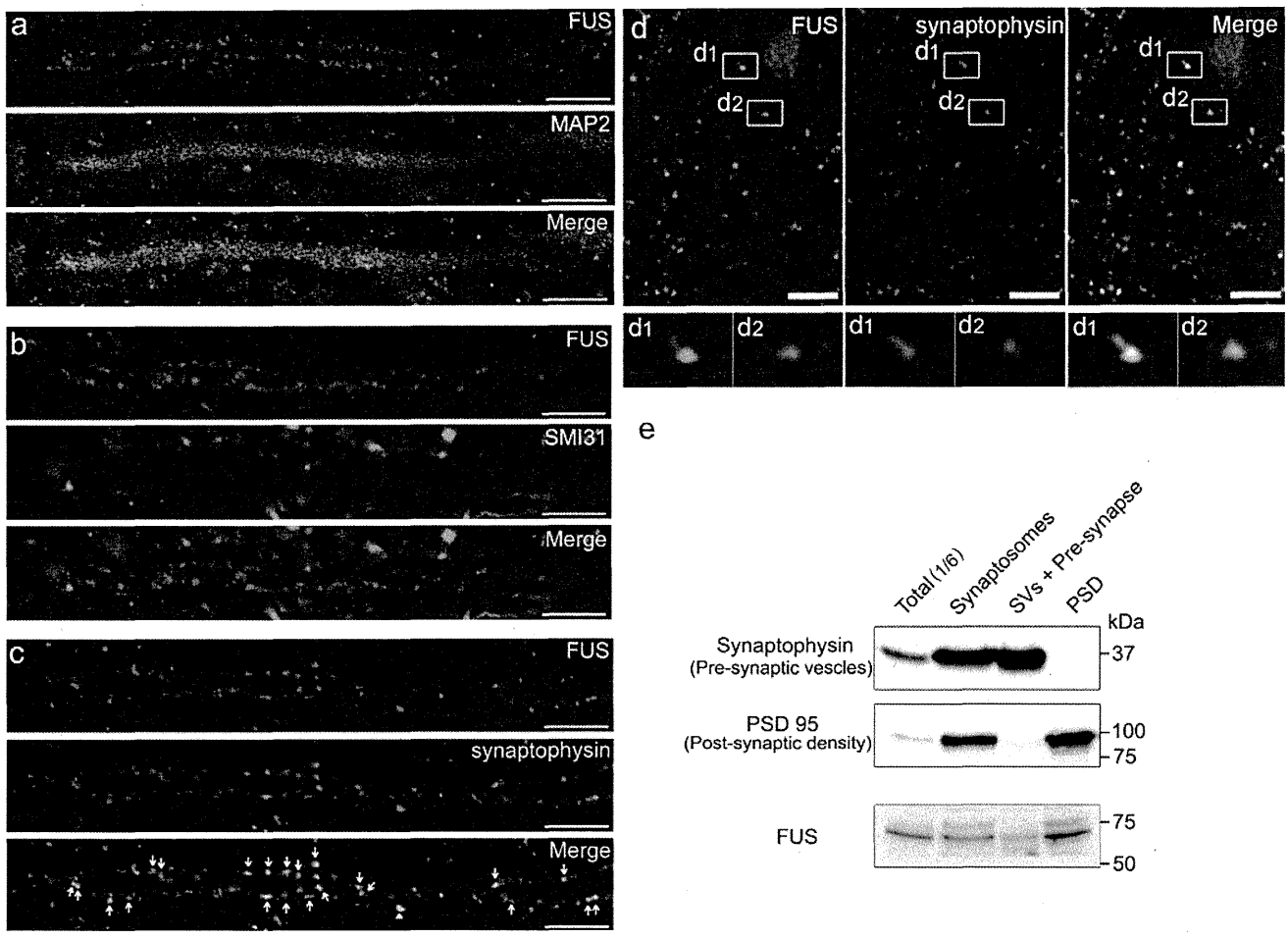

Fig. 6 **a–c** Confocal microscopic images of the substantia nigra pars compacta of a control subject. Double immunofluorescence staining for FUS and MAP-2 (**a**), FUS and phosphorylated neurofilament (**b**), and FUS and synaptophysin (**c**). FUS-positive granules are present along with MAP-2 positive dendrites (**a**) but are not associated with phosphorylated neurofilament positive axons (**b**). FUS-positive granules show close association or overlap with synaptophysin immunoreactivity (**c**, *small arrows*). **d** Double immunofluorescence staining of the pontine nucleus for FUS and synaptophysin. *Boxed areas* in **d** are enlarged in *d1* and *d2*. Scale bars in **a–d** are 10 μm. **e** Western blot of the subcellular fractions of mouse brain. The majority of synaptosomal FUS is sedimented to the post-synaptic density fraction, which is marked by *PSD95*

In western blots, FUS is recognized as a 72-kDa protein in all organs of mouse and in the human brain which is consistent with previous reports [23, 32]. The molecular weight of FUS, estimated from the amino acid sequence, is about 53 kDa, indicating that further studies are required to clarify the molecular composition of FUS [23]. In both human and mouse brain, we have also detected with two anti-FUS antibodies raised against the N-terminal region a minor band of 28 kDa. To date, any transcriptional variant corresponding to this protein species has not been found, according to the four *Homo sapiens* FUS variants in the NCBI database (NM_004960, NR_028388, NM_001170634 and NM_001170937). Moreover, the HPA-008784 antibody was raised against a FUS fragment which mostly includes the N-terminal QGSY-rich region (aa 86–213), the estimated molecular weight of which is about 22 kDa, but this antibody did not detect the 28 kDa band. Therefore, the origin of the 28 kDa band may not be the FUS protein, although the possibility remains that this band represents an N-terminal fragment of FUS.

The dendritic FUS was detected by all anti-FUS antibodies employed, but the staining intensity was different among the antibodies. Two antibodies raised against the middle region of FUS stained the neuropil granules more intensely than the other antibodies. However, given that all anti-FUS antibodies detected the 72-kDa band by western blot analyses, this may depend on a difference in accessibility to the epitopes of FUS molecule between the nucleus and the dendrites. Distinct molecular conformation or binding with other proteins, for example, could cause such a difference.

The dendritic FUS granules in the cerebral cortex are increased in patients with FTLD-TDP and, less markedly, in those with AD. Such findings suggest that the dendritic FUS in cortical neurons may be involved in some reactive or

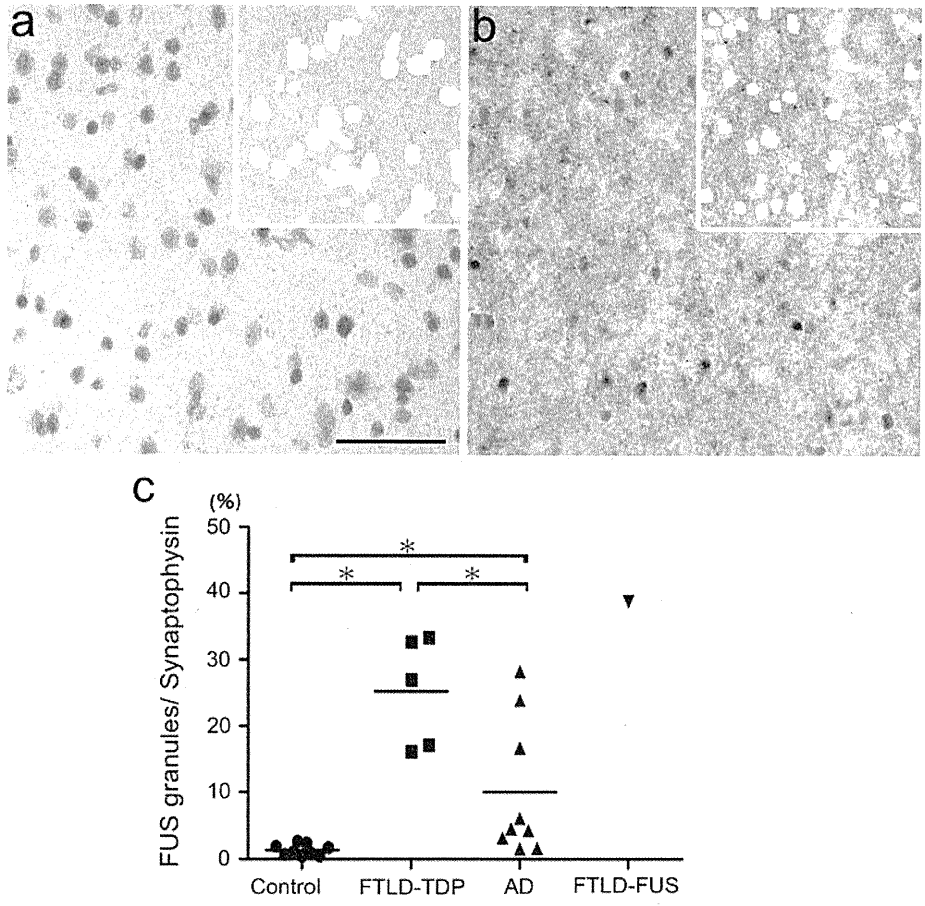

Fig. 7 Morphometric analyses of FUS-positive neuropil granules in the neocortex of the parahippocampal gyrus. Digital images were taken from FUS and haematoxylin-stained tissue sections of control subjects (**a**), FTLD-TDP patients Alzheimer's disease patients and an FTLD-FUS patient (**b**). Then, the nuclei were dissected out manually (**b** and **c**, *inset*) and the images were converted to a gray scale for quantitation. **c** FUS immunopositive pixels were counted and expressed as per cent of synaptophysin-positive pixels similarly counted in a nearby section. The results are shown as scatter plots. The *horizontal bars* indicate the mean values. $*p < 0.05$. The size of each image is 2,000 × 2,000 pixels. *Scale bar* 50 μm in **a**

degenerative change, in addition to its physiological functions. In a cell biologic study, FUS was shown to be recruited, in response to stress stimuli that lead to apoptosis, to stress granules, a form of cytoplasmic RNA granules that are composed of RNA-binding proteins and mRNA [8]. The increased dendritic FUS, therefore, might be associated with stress responses in neurodegenerative diseases. On the other hand, in a study with Drosophila models, cytoplasmic but not nuclear localization of FUS was linked to cellular degeneration [22]. The more pronounced increase in FTLD-TDP than in AD suggests its association with some abnormality in the dendritic RNA translation in which both FUS and TDP-43 are involved. In this study, only one FTLD-FUS case was available and, therefore, the significance of the result from this case remains uncertain. Nevertheless, an extreme increase of FUS granules in this case might support a notion that such a change is associated with the pathogenesis or pathophysiology of these RNA-binding protein-associated neurodegenerative diseases. Whether or not our observations are related to a recent finding that accumulation of FUS granules in the cytoplasm of spinal anterior horn cells in familial ALS with FUS mutations [25] is an issue of significant interest.

In conclusion, the immunohistochemical study of lightly fixed, free-floating sections of postmortem brains has revealed that FUS resides, not only in the nucleus, but also in the dendrites. At least, a portion of such FUS-immunoreactivity is located in the post-synapses. The specific neuroanatomical distribution, which is similar in mouse and human, indicates a physiological role, in particular, in the brainstem where the expression is mostly constitutive. The increase in the cerebral cortex in diseased brains infers that dendritic FUS is also related to some pathological processes.

Acknowledgments The authors thank the patients and their families who made this research possible. We also thank Dr. Kenichi Oshima and Dr. Kazuhiro Niizato (Tokyo Metropolitan Matuzawa Hospital), Dr. Eizo Iseki (Juntendo Tokyo Koto Geriatric Medical Center) and Dr. Mitsumoto Onaya (National Hospital Organization Shimofusa Psychiatric Medical Center) to provide brain samples. This research was supported by Grants-in-Aid for Young Scientists, 23791008 (S.H.) of the Japan Society for the Promotion of Science; Grants-in-Aid from the Ministry of Health, Labor and Welfare10102894 and 10103470 (H.A.), and the Ministry of Education, Culture, Science 09019658 (H.A.), Japan.

References

1. (1997) Consensus recommendations for the postmortem diagnosis of Alzheimer's disease. The National Institute on Aging, and Reagan Institute Working Group on Diagnostic Criteria for the

Neuropathological Assessment of Alzheimer's Disease. Neurobiol Aging 18:S1–S2
2. Andersson MK, Stahlberg A, Arvidsson Y, Olofsson A, Semb H, Stenman G, Nilsson O, Aman P (2008) The multifunctional FUS, EWS and TAF15 proto-oncoproteins show cell type-specific expression patterns and involvement in cell spreading and stress response. BMC Cell Biol 9:37
3. Arai T, Hasegawa M, Akiyama H, Ikeda K, Nonaka T, Mori H, Mann D, Tsuchiya K, Yoshida M, Hashizume Y, Oda T (2006) TDP-43 is a component of ubiquitin-positive tau-negative inclusions in frontotemporal lobar degeneration and amyotrophic lateral sclerosis. Biochem Biophys Res Commun 351:602–611
4. Arai T, Mackenzie IR, Hasegawa M, Nonoka T, Niizato K, Tsuchiya K, Iritani S, Onaya M, Akiyama H (2009) Phosphorylated TDP-43 in Alzheimer's disease and dementia with Lewy bodies. Acta Neuropathol 117:125–136
5. Armstrong RA, Gearing M, Bigio EH, Cruz-Sanchez FF, Duyckaerts C, Mackenzie IR, Perry RH, Skullerud K, Yokoo H, Cairns NJ (2011) The spectrum and severity of FUS-immunoreactive inclusions in the frontal and temporal lobes of ten cases of neuronal intermediate filament inclusion disease. Acta Neuropathol 121:219–228
6. Belly A, Moreau-Gachelin F, Sadoul R, Goldberg Y (2005) Delocalization of the multifunctional RNA splicing factor TLS/FUS in hippocampal neurones: exclusion from the nucleus and accumulation in dendritic granules and spine heads. Neurosci Lett 379:152–157
7. Bian H, Grossman M (2007) Frontotemporal lobar degeneration: recent progress in antemortem diagnosis. Acta Neuropathol 114:23–29
8. Bosco DA, Lemay N, Ko HK, Zhou H, Burke C, Kwiatkowski TJ Jr, Sapp P, McKenna-Yasek D, Brown RH Jr, Hayward LJ (2010) Mutant FUS proteins that cause amyotrophic lateral sclerosis incorporate into stress granules. Hum Mol Genet 19:4160–4175
9. Bouvier D, Corera AT, Tremblay ME, Riad M, Chagnon M, Murai KK, Pasquale EB, Fon EA, Doucet G (2008) Pre-synaptic and post-synaptic localization of EphA4 and EphB2 in adult mouse forebrain. J Neurochem 106:682–695
10. Cairns NJ, Bigio EH, Mackenzie IR, Neumann M, Lee VM, Hatanpaa KJ, White CL 3rd, Schneider JA, Grinberg LT, Halliday G, Duyckaerts C, Lowe JS, Holm IE, Tolnay M, Okamoto K, Yokoo H, Murayama S, Woulfe J, Munoz DG, Dickson DW, Ince PG, Trojanowski JQ, Mann DM (2007) Neuropathologic diagnostic and nosologic criteria for frontotemporal lobar degeneration: consensus of the Consortium for Frontotemporal Lobar Degeneration. Acta Neuropathol 114:5–22
11. Dormann D, Rodde R, Edbauer D, Bentmann E, Fischer I, Hruscha A, Than ME, Mackenzie IR, Capell A, Schmid B, Neumann M, Haass C (2010) ALS-associated fused in sarcoma (FUS) mutations disrupt transportin-mediated nuclear import. EMBO J 29:2841–2857
12. Fujii R, Okabe S, Urushido T, Inoue K, Yoshimura A, Tachibana T, Nishikawa T, Hicks GG, Takumi T (2005) The RNA binding protein TLS is translocated to dendritic spines by mGluR5 activation and regulates spine morphology. Curr Biol 15:587–593
13. Fujii R, Takumi T (2005) TLS facilitates transport of mRNA encoding an actin-stabilizing protein to dendritic spines. J Cell Sci 118:5755–5765
14. Geser F, Brandmeir NJ, Kwong LK, Martinez-Lage M, Elman L, McCluskey L, Xie SX, Lee VM, Trojanowski JQ (2008) Evidence of multisystem disorder in whole-brain map of pathological TDP-43 in amyotrophic lateral sclerosis. Arch Neurol 65:636–641
15. Gitcho MA, Baloh RH, Chakraverty S, Mayo K, Norton JB, Levitch D, Hatanpaa KJ, White CL 3rd, Bigio EH, Caselli R, Baker M, Al-Lozi MT, Morris JC, Pestronk A, Rademakers R, Goate AM, Cairns NJ (2008) TDP-43 A315T mutation in familial motor neuron disease. Ann Neurol 63:535–538
16. Hahn CG, Banerjee A, Macdonald ML, Cho DS, Kamins J, Nie Z, Borgmann-Winter KE, Grosser T, Pizarro A, Ciccimaro E, Arnold SE, Wang HY, Blair IA (2009) The post-synaptic density of human postmortem brain tissues: an experimental study paradigm for neuropsychiatric illnesses. PLoS ONE 4:e5251
17. Higashi S, Iseki E, Minegishi M, Togo T, Kabuta T, Wada K (2010) GIGYF2 is present in endosomal compartments in the mammalian brains and enhances IGF-1-induced ERK1/2 activation. J Neurochem 115:423–437
18. Higashi S, Moore DJ, Minegishi M, Kasanuki K, Fujishiro H, Kabuta T, Togo T, Katsuse O, Uchikado H, Furukawa Y, Hino H, Kosaka K, Sato K, Arai H, Wada K, Iseki E (2011) Localization of MAP1-LC3 in vulnerable neurons and Lewy bodies in brains of patients with dementia with Lewy bodies. J Neuropathol Exp Neurol 70:264–280
19. Iida J, Nishimura W, Yao I, Hata Y (2002) Synaptic localization of membrane-associated guanylate kinase-interacting protein mediated by the pleckstrin homology domain. Eur J Neurosci 15:1493–1498
20. Kabashi E, Valdmanis PN, Dion P, Spiegelman D, McConkey BJ, Vande Velde C, Bouchard JP, Lacomblez L, Pochigaeva K, Salachas F, Pradat PF, Camu W, Meininger V, Dupre N, Rouleau GA (2008) TARDBP mutations in individuals with sporadic and familial amyotrophic lateral sclerosis. Nat Genet 40:572–574
21. Kwiatkowski TJ Jr, Bosco DA, Leclerc AL, Tamrazian E, Vanderburg CR, Russ C, Davis A, Gilchrist J, Kasarskis EJ, Munsat T, Valdmanis P, Rouleau GA, Hosler BA, Cortelli P, de Jong PJ, Yoshinaga Y, Haines JL, Pericak-Vance MA, Yan J, Ticozzi N, Siddique T, McKenna-Yasek D, Sapp PC, Horvitz HR, Landers JE, Brown RH Jr (2009) Mutations in the FUS/TLS gene on chromosome 16 cause familial amyotrophic lateral sclerosis. Science 323:1205–1208
22. Lanson NA Jr, Maltare A, King H, Smith R, Kim JH, Taylor JP, Lloyd TE, Pandey UB (2011) A Drosophila model of FUS-related neurodegeneration reveals genetic interaction between FUS and TDP-43. Hum Mol Genet 20:2510–2523
23. Lashley T, Rohrer JD, Bandopadhyay R, Fry C, Ahmed Z, Isaacs AM, Brelstaff JH, Borroni B, Warren JD, Troakes C, King A, Al-Saraj S, Newcombe J, Quinn N, Ostergaard K, Schroder HD, Bojsen-Moller M, Braendgaard H, Fox NC, Rossor MN, Lees AJ, Holton JL, Revesz T (2011) A comparative clinical, pathological, biochemical and genetic study of fused in sarcoma proteinopathies. Brain 134:2548–2564
24. Liu-Yesucevitz L, Bassell GJ, Gitler AD, Hart AC, Klann E, Richter JD, Warren ST, Wolozin B (2011) Local RNA translation at the synapse and in disease. J Neurosci 31:16086–16093
25. Mackenzie IR, Ansorge O, Strong M, Bilbao J, Zinman L, Ang LC, Baker M, Stewart H, Eisen A, Rademakers R, Neumann M (2011) Pathological heterogeneity in amyotrophic lateral sclerosis with FUS mutations: two distinct patterns correlating with disease severity and mutation. Acta Neuropathol 122:87–98
26. Mackenzie IR, Munoz DG, Kusaka H, Yokota O, Ishihara K, Roeber S, Kretzschmar HA, Cairns NJ, Neumann M (2011) Distinct pathological subtypes of FTLD-FUS. Acta Neuropathol 121:207–218
27. Mackenzie IR, Neumann M, Baborie A, Sampathu DM, Du Plessis D, Jaros E, Perry RH, Trojanowski JQ, Mann DM, Lee VM (2011) A harmonized classification system for FTLD-TDP pathology. Acta Neuropathol 122:111–113
28. Mackenzie IR, Neumann M, Bigio EH, Cairns NJ, Alafuzoff I, Kril J, Kovacs GG, Ghetti B, Halliday G, Holm IE, Ince PG, Kamphorst W, Revesz T, Rozemuller AJ, Kumar-Singh S, Akiyama H, Baborie A, Spina S, Dickson DW, Trojanowski JQ, Mann DM (2009) Nomenclature for neuropathologic subtypes of

frontotemporal lobar degeneration: consensus recommendations. Acta Neuropathol 117:15–18
29. Mackenzie IR, Neumann M, Bigio EH, Cairns NJ, Alafuzoff I, Kril J, Kovacs GG, Ghetti B, Halliday G, Holm IE, Ince PG, Kamphorst W, Revesz T, Rozemuller AJ, Kumar-Singh S, Akiyama H, Baborie A, Spina S, Dickson DW, Trojanowski JQ, Mann DM (2010) Nomenclature and nosology for neuropathologic subtypes of frontotemporal lobar degeneration: an update. Acta Neuropathol 119:1–4
30. Munoz DG, Neumann M, Kusaka H, Yokota O, Ishihara K, Terada S, Kuroda S, Mackenzie IR (2009) FUS pathology in basophilic inclusion body disease. Acta Neuropathol 118:617–627
31. Neary D, Snowden JS, Gustafson L, Passant U, Stuss D, Black S, Freedman M, Kertesz A, Robert PH, Albert M, Boone K, Miller BL, Cummings J, Benson DF (1998) Frontotemporal lobar degeneration: a consensus on clinical diagnostic criteria. Neurology 51:1546–1554
32. Neumann M, Rademakers R, Roeber S, Baker M, Kretzschmar HA, Mackenzie IR (2009) A new subtype of frontotemporal lobar degeneration with FUS pathology. Brain 132:2922–2931
33. Neumann M, Roeber S, Kretzschmar HA, Rademakers R, Baker M, Mackenzie IR (2009) Abundant FUS-immunoreactive pathology in neuronal intermediate filament inclusion disease. Acta Neuropathol 118:605–616
34. Neumann M, Sampathu DM, Kwong LK, Truax AC, Micsenyi MC, Chou TT, Bruce J, Schuck T, Grossman M, Clark CM, McCluskey LF, Miller BL, Masliah E, Mackenzie IR, Feldman H, Feiden W, Kretzschmar HA, Trojanowski JQ, Lee VM (2006) Ubiquitinated TDP-43 in frontotemporal lobar degeneration and amyotrophic lateral sclerosis. Science 314:130–133
35. Prasad DD, Ouchida M, Lee L, Rao VN, Reddy ES (1994) TLS/FUS fusion domain of TLS/FUS-erg chimeric protein resulting from the t(16;21) chromosomal translocation in human myeloid leukemia functions as a transcriptional activation domain. Oncogene 9:3717–3729
36. Ringholz GM, Appel SH, Bradshaw M, Cooke NA, Mosnik DM, Schulz PE (2005) Prevalence and patterns of cognitive impairment in sporadic ALS. Neurology 65:586–590
37. Rosso SM, Donker Kaat L, Baks T, Joosse M, de Koning I, Pijnenburg Y, de Jong D, Dooijes D, Kamphorst W, Ravid R, Niermeijer MF, Verheij F, Kremer HP, Scheltens P, van Duijn CM, Heutink P, van Swieten JC (2003) Frontotemporal dementia in The Netherlands: patient characteristics and prevalence estimates from a population-based study. Brain 126:2016–2022
38. Sreedharan J, Blair IP, Tripathi VB, Hu X, Vance C, Rogelj B, Ackerley S, Durnall JC, Williams KL, Buratti E, Baralle F, de Belleroche J, Mitchell JD, Leigh PN, Al-Chalabi A, Miller CC, Nicholson G, Shaw CE (2008) TDP-43 mutations in familial and sporadic amyotrophic lateral sclerosis. Science 319:1668–1672
39. The Lund and Manchester Groups (1994) Clinical and neuropathological criteria for frontotemporal dementia. J Neurol Neurosurg Psychiatry 57:416–418
40. Van Deerlin VM, Leverenz JB, Bekris LM, Bird TD, Yuan W, Elman LB, Clay D, Wood EM, Chen-Plotkin AS, Martinez-Lage M, Steinbart E, McCluskey L, Grossman M, Neumann M, Wu IL, Yang WS, Kalb R, Galasko DR, Montine TJ, Trojanowski JQ, Lee VM, Schellenberg GD, Yu CE (2008) TARDBP mutations in amyotrophic lateral sclerosis with TDP-43 neuropathology: a genetic and histopathological analysis. Lancet Neurol 7:409–416
41. Vance C, Rogelj B, Hortobagyi T, De Vos KJ, Nishimura AL, Sreedharan J, Hu X, Smith B, Ruddy D, Wright P, Ganesalingam J, Williams KL, Tripathi V, Al-Saraj S, Al-Chalabi A, Leigh PN, Blair IP, Nicholson G, de Belleroche J, Gallo JM, Miller CC, Shaw CE (2009) Mutations in FUS, an RNA processing protein, cause familial amyotrophic lateral sclerosis type 6. Science 323:1208–1211
42. Wang HY, Wang IF, Bose J, Shen CK (2004) Structural diversity and functional implications of the eukaryotic TDP gene family. Genomics 83:130–139
43. Yokoseki A, Shiga A, Tan CF, Tagawa A, Kaneko H, Koyama A, Eguchi H, Tsujino A, Ikeuchi T, Kakita A, Okamoto K, Nishizawa M, Takahashi H, Onodera O (2008) TDP-43 mutation in familial amyotrophic lateral sclerosis. Ann Neurol 63:538–542
44. Zinszner H, Sok J, Immanuel D, Yin Y, Ron D (1997) TLS (FUS) binds RNA in vivo and engages in nucleo-cytoplasmic shuttling. J Cell Sci 110:1741–1750

Brain Advance Access published October 3, 2012
doi:10.1093/brain/aws230

BRAIN
A JOURNAL OF NEUROLOGY

Molecular analysis and biochemical classification of TDP-43 proteinopathy

Hiroshi Tsuji,[1,2] Tetsuaki Arai,[3,4] Fuyuki Kametani,[1] Takashi Nonaka,[1] Makiko Yamashita,[1] Masami Suzukake,[1] Masato Hosokawa,[3] Mari Yoshida,[5] Hiroyuki Hatsuta,[6] Masaki Takao,[6] Yuko Saito,[7] Shigeo Murayama,[6] Haruhiko Akiyama,[3] Masato Hasegawa,[1] David M. A. Mann[8] and Akira Tamaoka[2]

1 Department of Neuropathology and Cell Biology, Tokyo Metropolitan Institute of Medical Science, Tokyo 156-8585, Japan
2 Department of Neurology, Graduate School of Comprehensive Human Sciences, University of Tsukuba, Tsukuba-shi 305-8576, Japan
3 Department of Dementia and Higher Brain Function, Tokyo Metropolitan Institute of Medical Science, Tokyo 156-8585, Japan
4 Department of Psychiatry, Graduate School of Comprehensive Human Sciences, University of Tsukuba, Tsukuba-shi 305-8576, Japan
5 Department of Neuropathology, Institute for Medical Science of Aging, Aichi Medical University, Aichi 480-1195, Japan
6 Department of Neuropathology, Tokyo Metropolitan Institute of Gerontology, Tokyo 173-0015, Japan
7 Department of Pathology and Laboratory Medicine, National Center Hospital of Neurology and Psychiatry, Tokyo 187-8551, Japan
8 Mental Health and Neurodegeneration Research Group, Greater Manchester Neuroscience Centre, University of Manchester, Manchester M13 9PT, UK

Correspondence to: Masato Hasegawa,
Department of Neuropathology and Cell Biology,
Tokyo Metropolitan Institute of Medical Science,
2-1-6 Kamikitazawa,
Setagaya-ku,
Tokyo 156-8506,
Japan
E-mail: hasegawa-ms@igakuken.or.jp

Amyotrophic lateral sclerosis and frontotemporal lobar degeneration with TAR DNA-binding protein of 43 kDa pathology are progressive neurodegenerative diseases that are characterized by intracytoplasmic aggregates of hyperphosphorylated TAR DNA-binding protein of 43 kDa. These TAR DNA-binding protein 43 proteinopathies can be classified into subtypes, which are closely correlated with clinicopathological phenotypes, although the differences in the molecular species of TAR DNA-binding protein 43 in these diseases and the biological significance thereof, remain to be clarified. Here, we have shown that although the banding patterns of abnormally phosphorylated C-terminal fragments of TAR DNA-binding protein 43 differ between the neuropathological subtypes, these are indistinguishable between multiple brain regions and spinal cord in individual patients. Immunoblot analysis of protease-resistant TAR DNA-binding protein 43 demonstrated that the fragment patterns represent different conformations of TAR DNA-binding protein 43 molecular species in the diseases. These results suggest a new clinicopathological classification of TAR DNA-binding protein 43 proteinopathies based on their molecular properties.

Keywords: amyotrophic lateral sclerosis; frontotemporal lobar degeneration; TDP-43; classification

Abbreviations: ALS = amyotrophic lateral sclerosis; FTLD = frontotemporal lobar degeneration; FTLD-TDP = frontotemporal lobar degeneration with TAR DNA-binding protein of 43 kDa pathology; TDP-43 = TAR DNA-binding protein of 43 kDa

Received March 13, 2012. Revised June 3, 2012. Accepted June 28, 2012

Introduction

Amyotrophic lateral sclerosis (ALS) and frontotemporal lobar degeneration with TDP-43 pathology (FTLD-TDP) are sporadic and familial neurodegenerative diseases characterized neuropathologically by intracytoplasmic aggregates of TAR DNA-binding protein of 43 kDa (TDP-43) (Arai *et al.*, 2006; Neumann *et al.*, 2006). In ALS, upper and lower motor neurons progressively degenerate. Neuropathologically, the TDP-43-positive structures appear as rounded or skein-like inclusions in the lower motor neurons. Similar TDP-43-positive inclusions are also observed in the prefrontal gyrus that contains the upper motor neurons. Moreover, TDP-43-positive glial cytoplasmic inclusions are found close to the upper and lower motor neurons in ALS (Tan *et al.*, 2007). In FTLD-TDP, TDP-43 pathology is distinguished into four histological subtypes (types A–D) based on the predominant type of TDP-43-positive structures present (Mackenzie *et al.*, 2011). Type A is characterized by numerous short dystrophic neurites and crescentic or oval neuronal cytoplasmic inclusions; type B has moderate numbers of neuronal cytoplasmic inclusions, throughout all cortical layers, but few dystrophic neurites; type C has a predominance of elongated dystrophic neurites in upper cortical layers, with few neuronal cytoplasmic inclusions; and type D refers to the pathology associated with inclusion body myopathy with early onset Paget disease and frontotemporal dementia caused by *VCP* mutations, characterized by numerous short dystrophic neurites and frequent lentiform neuronal intranuclear inclusions. There is a relationship between subtypes of TDP-43 pathology and clinical phenotype, and many cases of ALS and frontotemporal lobar degeneration (FTLD) are readily distinguished by each clinical symptom. However, some cases have symptoms of both ALS and FTLD. ALS with dementia refers to cases initially presenting with motor neuron disease becoming demented, whereas FTLD-motor neuron disease refers to cases presenting with cognitive impairment and subsequently developing motor neuron disease.

TDP-43 pathology is also present in a subset of familial ALS and FTLD due to mutations in *TARDBP* (Kabashi *et al.*, 2008; Sreedharan *et al.*, 2008), progranulin (*GRN*; Baker *et al.*, 2006) and *C9ORF72* (DeJesus-Hernandez *et al.*, 2011; Renton *et al.*, 2011) genes. Although most patients with mutations in *TARDBP* present with ALS, some present with FTLD (Gitcho *et al.*, 2009; Kovacs *et al.*, 2009). Cases with FTLD-TDP with *GRN* mutation often show type A pathology (Mackenzie *et al.*, 2006b; Cairns *et al.*, 2007b; Josephs *et al.*, 2007). The pathology of ALS and FTLD due to mutations in *C9ORF72* is heterogeneous: TDP-43 pathology overlaps between ALS and FTLD-TDP types A and B (Murray *et al.*, 2011). One large multicentre study of sporadic and familial FTLD-TDP showed broad overlap between the TDP-43 subtyping, especially between types A and B (Armstrong *et al.*, 2010). These overlaps might occur because current pathological classification may be inadequate, as it is based solely on the morphological assessment of certain subjective cortical regions. A more objective and unbiased classification is needed.

In this study, we have investigated a wide range of patients with various TDP-43 proteinopathies to investigate whether patterns of protease-resistant TDP-43 might indicate different TDP-43 strain types, and characterize the TDP-43 C-terminal banding patterns in multiple regions of the CNS, basing our approach on the method used for demonstration of prion strain variation and the aetiology of new variant Creutzfeldt–Jakob disease (Collinge *et al.*, 1996). We show at least three C-terminal banding patterns that distinguish diseases with TDP-43 proteinopathy and report that the banding pattern in individual patients is indistinguishable in different brain regions and spinal cord. Corresponding patterns of protease-resistant phosphorylated TDP-43 are also seen between the pathological phenotypes. As with the prion diseases, the present results suggest that the different conformation of abnormal TDP-43 deposits in the CNS in patients corresponding with various subtypes of TDP-43 proteinopathy, and that the conformation state of the abnormal TDP-43 protein may determine the pathological phenotype.

Materials and methods

Patients

Human brain tissues were obtained from the Brain Donation Programme at the University of Tsukuba (Japan), Tokyo Metropolitan Institute of Gerontology (Japan), National Shimofusa Mental Hospital (Japan) and the University of Manchester (UK). This study was approved by the local Research Ethics Committee. The subjects in this study included eight patients with ALS, five patients with FTLD-TDP type A, eight patients with FTLD-TDP type B, six patients with FTLD-TDP type C and two patients with Alzheimer's disease without TDP-43 pathology. All cases with ALS met the revised El Escorial criteria for ALS (Brooks, 1994) without dementia. All cases with FTLD-TDP fulfilled clinical diagnostic criteria of FTLD (Neary *et al.*, 1998), and classifications of TDP-43 subtype were made in accordance with published guidelines (Cairns *et al.*, 2007a; Mackenzie *et al.*, 2011). Four patients with FTLD-TDP type A were cases of familial FTLD-U with *GRN* mutations. One familial ALS case, one with type A, and two with type B had the GGGCC repeat expansion in *C9ORF72*. The age, gender, brain regions examined and clinical diagnosis are given in Table 1.

A fresh frozen tissue sample was taken and cut into two pieces. One piece was fixed in 4% paraformaldehyde in 0.1 M phosphate buffer (pH 7.4) for 2 days and was used for immunohistochemical analysis. The other piece was homogenized and used for immunoblot analysis. In principle, we took the precentral gyrus and lumbar part of the spinal cord in the ALS cases, and the frontal lobe in the FTLD-TDP cases, because TDP-43 pathology is always known to be prevalent in these regions (Tan *et al.*, 2007; Geser *et al.*, 2008, 2009). However, the spinal cord was not available in four cases with ALS, and both motor regions in two cases were not available. In these cases, the frontal lobe was examined instead. For ALS Cases 1, 3, 5 and ALS and FTLD-TDP type C Case 22, the whole of the cerebral hemisphere and brainstem were available as fresh frozen tissues. In these four cases, we took the multiple regions, as described in Table 1. Every tissue sample was examined immunohistochemically for TDP-43-positive lesions. All samples, except some from the cerebellar cortex, showed an accumulation of abnormal TDP-43-positive structures.

Immunoblotting

Sarkosyl-insoluble, urea-soluble fractions were extracted from each region as previously described (Arai *et al.*, 2006; Hasegawa *et al.*, 2008).

Table 1 Description of the patients

Case number	Age at death (year)	Age at onset (year)	Sex	Family history	Brain weight (g)	Clinical diagnosis	Region
ALS							
1	62	61	M	N	1150	ALS	Prec, L and other regions[a]
2	72	71	F	N	1390	ALS	Prec and L
3	42	40	F	N	1140	ALS	Prec, L and other regions[a]
4	76	75	F	N	NA	ALS	Prec and L
5	62	54	M	N	1230	ALS	Prec and other regions[a]
6	77	76	F	N	NA	ALS	Prec
7	67	65	M	N	1414	ALS	Fr
8	55	53	M	Y(m*C9ORF72*)	1250	ALS	Fr
FTLD-TDP type A							
9	58	49	M	Y(m*C9ORF72*)	1050	FTD	Fr
10	67	54	F	Y(m*GRN*)	NA	FTD	Fr
11	71	63	F	Y(m*GRN*)	863	PNFA	Fr
12	66	56	F	Y(m*GRN*)	1100	FTD	Fr
13	68	60	M	Y(m*GRN*)	1210	FTD + MND	Fr
FTLD-TDP type B							
14	45	43	M	N	1260	FTD + MND	Fr
15	59	57	M	Y(m*C9ORF72*)	1210	FTD + MND	Fr
16	67	65	M	N	1280	FTD + MND	Fr
17	76	74	M	N	1215	FTD + MND	Fr
18	69	58	M	N	1166	FTD + MND	Fr
19	52	50	F	Y(m*C9ORF72*)	1050	FTD + MND	Fr
20	65	61	M	N	1530	FTD + MND	Fr
21	68	64	M	N	1213	FTD + MND	Fr
FTLD-TDP type C							
22	82	NA	M	N	1200	SD	Fr, Te and other regions[b]
23	67	65	M	N	NA	SD	Fr
24	59	53	M	N	NA	SD	Fr
25	63	58	M	N	NA	SD	Fr
26	66	55	F	N	1035	SD	Fr
27	75	60	M	N	1174	SD	Fr
AD							
28	65	56	F	N	1165	AD	Fr
29	70	NA	F	N	1126	AD	Fr

AD = Alzheimer's disease; Fr = frontal cortex; FTD = frontotemporal dementia; L = lumbar part of spinal cord; m*C9ORF72* = mutation of chromosome 9 open-reading frame 72 gene; m*GRN* = mutation of progranulin gene; MND = motor neuron disease; NA = not available; PNFA = progressive non-fluent aphasia; Prec = precentral gyrus; SD = semantic dementia; Y = yes; N = no.

a Other regions contained striatum, thalamus, hippocampus dentate gyrus, substantia nigra, pons, medulla and cerebellum cortex. In these cases, the grey and white matter of precentral gyrus were separated from each other macroscopically and examined.

b Other regions contain striatum, thalamus, hippocampus dentate gyrus, substantia nigra, pons, medulla and cerebellum cortex. FTLD-TDP type B without MND and type D are not analysed in this study.

The samples were loaded on 15% SDS–PAGE gels. Proteins in the gel were then transferred onto a polyvinylidene difluoride membrane (Millipore). After blocking with 3% gelatine in 0.01 M PBS (pH 7.4), membranes were incubated overnight with phosphorylation dependent anti-TDP-43 rabbit polyclonal antibody (pS409/410, 1:1000; Hasegawa *et al.*, 2008), phosphorylation independent TDP-43 polyclonal antibody 10782-1-AP (TDP-43 pAb, 1:3000) and TDP-43 monoclonal antibody, 60019-2-Ig (TDP-43 mAb, 1:3000) (ProteinTech Group). After incubation with the appropriate biotinylated secondary antibody, immunolabelling was detected using the VECTASTAIN® ABC system (Vector Laboratories) coupled with a 3,3′-diaminobenzidine reaction intensified with nickel chloride. The blot membranes were digitally analysed, and densitometric analyses were performed with ImageJ version 1.44p (NIH, http://rsbweb.nih.gov/ij/index.html). The densitometry data were averaged for all cases in each group to illustrate the different patterns.

Immunohistochemistry

After cryoprotection in 15% sucrose in 0.01 M PBS (pH 7.4), paraformaldehyde-fixed tissue blocks were cut on a freezing microtome at 30-μm thickness. The free-floating sections were immunostained with phosphorylation-dependent TDP-43 monoclonal antibody (pS409/410, 1:10 000) (Inukai *et al.*, 2008) for 72 h in the cold. After treatment with mouse secondary antibody, immunolabelling was detected using the VECTASTAIN ®ABC system coupled with a 3,3′-diaminobenzidine reaction to yield a brown precipitate. Sections were lightly counterstained with heamatoxylin.

Protease treatment of phosphorylated TDP-43

Sarkosyl-insoluble fractions extracted from the neocortical regions of patients with ALS or FTLD-TDP were treated with final concentration of 100 μg/ml trypsin (Promega) or 10 μg/ml chymotrypsin (Sigma-Aldrich) at 37°C for 30 min. The reaction was stopped by boiling for 5 min. After centrifuging at 15 000 rpm for 1 min, the samples were analysed by immunoblotting as described earlier.

Mass spectrometry

Sarkosyl-insoluble, trypsin-resistant fractions were loaded on 15% SDS–PAGE gels. The pS409/410-positive ~16 kDa bands were dissected and digested in-gel with chymotrypsin. The digests were applied to the Paradigm MS4 high-performance liquid chromatography system (Microm BioResources). A reversed phase capillary column (Develosil ODS-HG5, 0.075 × 150 mm, Nomura Chemical) was used at a flow rate of 300 nl/min with a 4–80% linear gradient of acetonitrile in 0.1% formic acid. Eluted peptides were directly detected with an ion trap mass spectrometer, LXQ (Thermo Fisher Scientific). The obtained spectra were analysed with Mascot (Matrix Science).

Statistical analysis

The *P*-values for the description of the statistical significance of differences were calculated by means of the paired, two-tailed *t*-test using Prism 5.04 software (GraphPad Software, Inc).

Results

Banding patterns of phosphorylated C-terminal TDP-43 in ALS and FTLD with TDP-43 pathology

Immunoblot analysis using an antibody specific for abnormal TDP-43, pS409/410, showed high-molecular-weight smearing substances, phosphorylated full-length TDP-43 at 45 kDa and several C-terminal fragments at 18–26 kDa to be present in affected brain regions in all cases (Fig. 1). Three major bands at 23, 24 and 26 kDa, and two minor bands at 18 and 19 kDa were seen in the precentral gyrus and frontal cortex of cases with ALS, with the 24 kDa band being the most intense (Fig. 1A and F). In the lumbar spinal cord, the two minor bands at 18 and 19 kDa were barely present, but the banding pattern of the three major bands at 23, 24 and 26 kDa was similar to that in the cerebral cortex (Fig. 1A). No such pS409/410-positive TDP-43 bands were detected in control cases with Alzheimer's disease with no TDP-43 pathology (Fig. 1B). In the FTLD-TDP cases, the banding pattern could be distinguished into three types according to the FTLD-TDP histological subtype (Fig. 1C–E). In FTLD-TDP type A, three major bands at 23, 24 and 26 kDa, and two minor bands at 18 and 19 kDa were detected, with the 23 kDa band being the most intense (Fig. 1C and F). In FTLD-type B cases, the banding pattern was the same as that in the ALS cases (Fig. 1D and F). In FTLD-TDP type C cases, two major bands at 23 and 24 kDa, and two minor bands at 18 and 19 kDa were detected, with the 24 kDa band being the most intense, and the band at 26 kDa being hardly detectable (Fig. 1E and F). Densitometric analyses of the immunoblots for all cases are shown in Supplementary Fig. 1. Each component of the C-terminal fragments was significantly different (Fig. 1F).

Immunoblot analysis using phosphorylation independent TDP-43 polyclonal and monoclonal antibodies detected phosphorylated full-length TDP-43 at 45 kDa, two bands ~25 kDa and high-molecular-weight smears, in addition to the normal TDP-43 band at 43 kDa in ALS and various subtypes of FTLD-TDP. The banding patterns between ALS and various subtypes of FTLD-TDP could not be distinguished with these antibodies. In the cases with Alzheimer's disease, the normal TDP-43 band at 43 kDa was detected, but neither the phosphorylated 45 kDa band nor the ~25 kDa fragments were observed (Supplementary Fig. 2). Immunoblot analysis of α-tubulin in Tris saline-soluble fractions from cases with types A, B and C pathology showed no correlation between the banding pattern of α-tubulin and that of TDP-43 (Supplementary Fig. 3), indicating that the differences in the banding patterns are not because of protein degradation caused by a long post-mortem interval or unfavourable agonal status.

Immunohistochemistry and immunoblot analyses of phosphorylated TDP-43 in multiple regions of ALS and FTLD with TDP-43 pathology

In ALS cases, the neuronal cytoplasmic pathology, which included skein-like inclusions, irregularly shaped TDP-immunoreactive neuronal cytoplasmic inclusions and densely staining granules, was confirmed in multiple regions by immunohistochemistry analysis using pS409/410 (Fig. 2A–G). Glial cytoplasmic inclusions were also present in many regions. Glial cytoplasmic inclusions were more frequent in the white matter than in the grey matter (Fig. 2H). A few neuronal cytoplasmic inclusions were found in the cerebellar cortex granule cells (Fig. 2G). In FTLD-TDP type C, dystrophic neurites were seen in multiple regions except for the cerebellar cortex (Fig. 2I–O), whereas neuronal cytoplasmic inclusions were also present in the striatum and hippocampus dentate gyrus granule cells (Fig. 2J and L). No abnormal structures were found in the cerebellar cortex (data not shown). These observations show that pathological TDP-43 is present throughout many CNS areas in ALS, suggesting that ALS does not selectively affect only the motor system, but it is rather a multisystem neurodegenerative TDP-43 proteinopathy.

Immunoblot analyses of three ALS cases confirmed that phosphorylated TDP-43 and the C-terminal fragments are deposited in multiple brain regions in ALS (Fig. 3A). Relatively strong immunoreactivities were detected in the striatum (in Cases 3 and 5) and substantia nigra (in Cases 1 and 5), although this varied between cases (Fig. 3A). Importantly, the banding pattern for the TDP-43 C-terminal fragments in these three cases was basically the same in all brain regions examined (Fig. 3A). In FTLD-TDP type C, a C-terminal banding pattern, clearly distinct from that

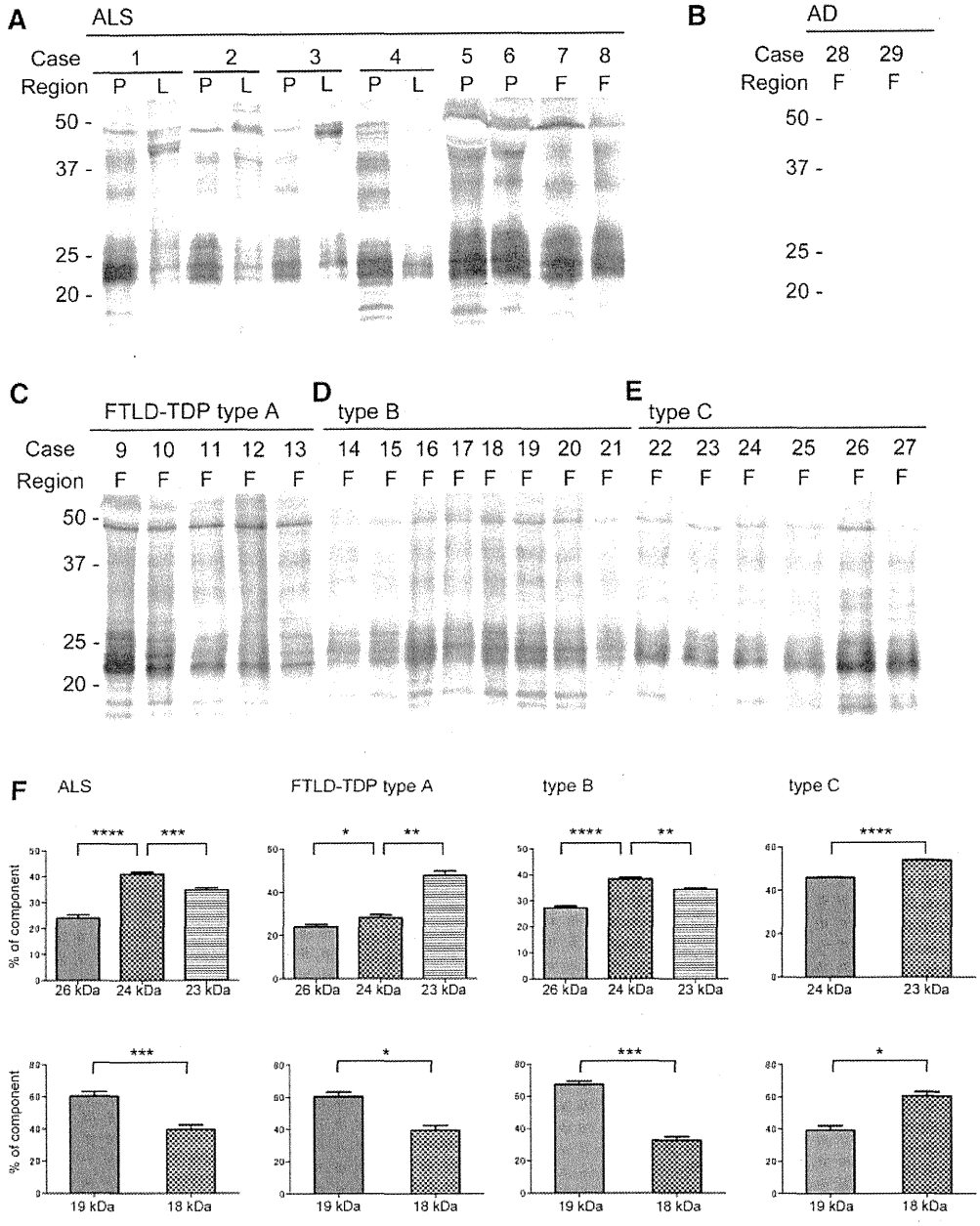

Figure 1 Immunoblot analyses of sarkosyl-insoluble TDP-43 in the brains or spinal cords of ALS (Cases 1–8) (**A**), Alzheimer's disease (Cases 28–29) (**B**), FTLD-TDP type A (Cases 9–13) (**C**), FTLD-TDP type B (Cases 14–21) (**D**) and FTLD-TDP type C (Cases 22–27) (**E**), using a phosphorylation-dependent anti-TDP-43 antibody (pS409/410). In all cases, high-molecular-weight smearing substances, phosphorylated full-length TDP-43 at 45 kDa and several C-terminal fragments at 18–26 kDa are detected. In ALS (**A**) and FTLD-TDP type B (**D**) cases, three major bands at 23, 24 and 26 kDa and two minor bands at 18 and 19 kDa are detected, whereas in the FTLD-TDP Type C (**E**) cases, two major bands at 23 and 24 and two minor bands at 18 and 19 kDa. A 24 kDa band is the most intense in ALS (**A**) and FTLD-TDP type B (**E**), whereas a 23 kDa band is the most intense in FTLD-TDP type C (**D**). The band pattern of the cases with type A (**C**) is an intermediate between FTLD-TDP type B (**D**) and FTLD-TDP type C (**E**). In spinal cords of cases with ALS, the 18 and 19 kDa bands are hardly detectable, but the same banding pattern of the 23–26 kDa bands as in precentral gyrus is detected. No such TDP-43 fragments are detected in brains of patients with Alzheimer's disease (AD) (**B**). The intensity of each C-terminal band was analysed using the ImageJ software and each component was statistically analysed by Student's *t*-test (**F**). Data indicate mean (SEM). $^{****}P < 0.0001$, $^{***}P < 0.001$, $^{**}P < 0.01$, $^{*}P < 0.05$. F = frontal cortex; L = lumbar part of spinal cord; P = precentral cortex.

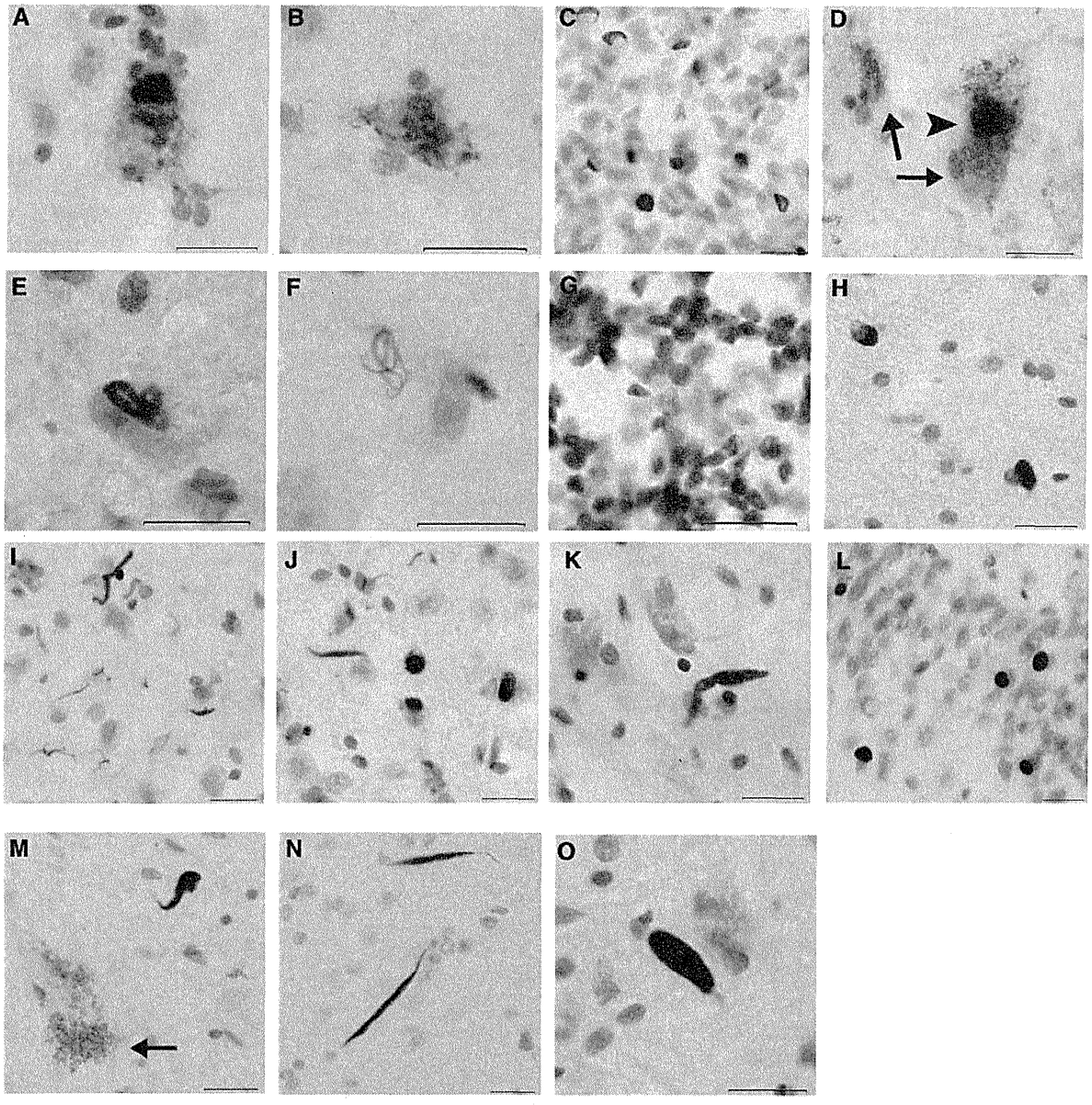

Figure 2 Phosphorylated TDP-43-positive structures observed in different brain regions and spinal cords of ALS (**A–H**) and FTLD-type C (**I–O**) using a phosphorylation-dependent anti-TDP-43 antibody (pS409/410). (**A**) Lewy body-like inclusion in the striatum neuron. (**B**) Cytoplasmic granular staining in the thalamus. (**C**) Neuronal cytoplasmic inclusions in the granular cells of hippocampus. (**D**) Irregularly shaped TDP-immunoreactive neuronal cytoplasmic inclusion in the substantia nigra (arrowhead). The arrows denote neuromelanin granules. (**E**) Skein-like inclusion in the motor nucleus of trigeminal nerve of pons. (**F**) Skein-like inclusion in the inferior olivary nucleus of medulla. (**G**) Neuronal cytoplasmic inclusion in the granular cells of cerebellar cortex. (**H**) Glial cytoplasmic inclusions in the white matter of precentral cortex. (**I**) Dystrophic neurites in the temporal cortex, (**J**) dystrophic neurites and neuronal cytoplasmic inclusions in the striatum. (**K**) Dystrophic neurites in the thalamus. (**L**) Neuronal cytoplasmic inclusions in the granular cells of hippocampus. (**M**) Dystrophic neurites in the substantia nigra. The arrow denotes neuromelanin granules. (**N**) Dystrophic neurites in the pons. (**O**) Dystrophic neurites in the medullary reticular formation. Scale bars = 20 μm.

of ALS, was detected in the temporal cortex, striatum and hippocampus, but was barely detected in the thalamus, substantia nigra, pons and medulla, and not at all in the cerebellar cortex (Fig. 3B). The banding pattern observed in these brain regions was indistinguishable (Fig. 3B). These results suggest that the same abnormal TDP-43 molecular species is deposited in different brain regions and different cell types, although the morphology of the TDP-43 inclusions may be different in the brain regions. Densitometric analyses of the immunoblots for all cases are shown in Supplementary Fig. 4.

Protease-resistant TDP-43 in ALS and FTLD with frontotemporal dementia-43 pathology

These different banding patterns in TDP-43 proteinopathies may represent different conformations of abnormal TDP-43 or their aggregates. To test this hypothesis, we subjected the abnormal TDP-43 recovered in the sarkosyl-insoluble pellets to protease treatment and analysed the protease-resistant bands. Proteins can be easily cleaved by proteases if they are denatured or unstructured, but domains that have rigid structures, such as a β-sheet conformation or that are structurally buried or interacting with other molecules, are highly resistant to proteases. On trypsin or chymotrypsin treatment, the full-length 45-kDa band and the smearing substance of TDP-43 disappeared, leaving protease-resistant fragments at 16–25 kDa (Figs 4 and 5). As expected, the protease-resistant banding patterns were different and distinguishable into three patterns (Figs 4 and 5). In ALS, trypsin-resistant doublet bands at 16 and 15 kDa, and two minor bands at ~24 kDa were detected, whereas a single band at 16 kDa and some additional bands at ~24 kDa were detected in FTLD-TDP type A (Fig. 4A, Lanes 1 and 2). In FTLD-TDP type B, the same banding pattern as that in ALS was observed (Fig. 4A, Lane 3). In FTLD-TDP type C, a broad single band at 16 kDa and some additional bands at ~24 kDa were detected (Fig. 4A, Lane 4). No such bands were detected in Alzheimer's disease (Fig. 4A, Lane 5).

Similarly, on chymotrypsin treatment, multiple protease-resistant bands were detected at 16–25 kDa and the chymotrypsin-resistant band patterns were also different between the three disease subtypes (Fig. 4B). Doublet bands were seen in ALS and FTLD-TDP type B, but only a single band in FTLD-TDP type C was detected at ~16 kDa (Fig. 4B). In FTLD-TDP type A, the lower band (15 kDa) of the ~16 kDa doublet was more intense than the upper one (16 kDa).

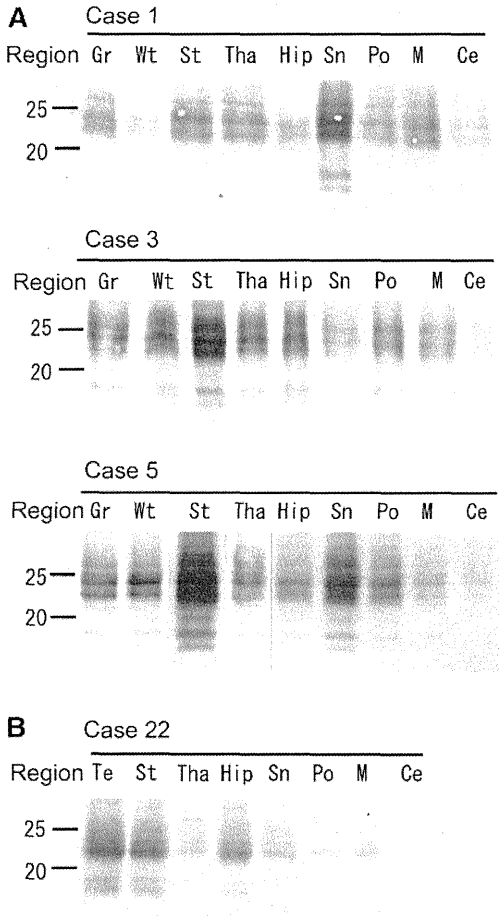

Figure 3 Immunoblot analyses of the C-terminal fragments of phosphorylated TDP-43 in the different brain regions of cases with ALS (Cases 1, 3 and 5, as shown in Fig. 1) (**A**) and FTLD-type C (Case 22, as shown in Fig. 1) (**B**). (**A**) Immunoblots of insoluble TDP-43 in the grey or white matter of precentral cortex, striatum, thalamus, hippocampus, substantia nigra, pons and medulla of ALS cases. (**B**) Immunoblot of TDP-43 in temporal cortex, striatum, hippocampus, thalamus, substantia nigra, pons and cerebellar cortex of the case with FTLD-TDP type C. Ce = Cerebellar cortex; Gr = grey matter of precentral gyrus; Hip = hippocampus; M = medulla; Po = pons; Sn = substantia nigra; St = striatum; Tha = thalamus; Te = temporal cortex; Wt = white matter of precentral gyrus. Immunoblots of spinal cords of cases with ALS are shown in Fig. 1.

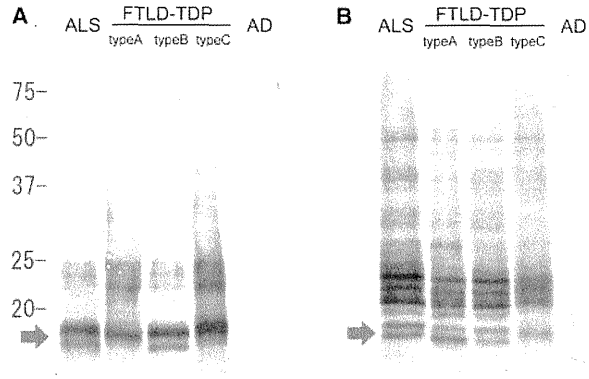

Figure 4 Immunoblot analysis of phosphorylated TDP-43 from representative ALS and FTLD-TDP cases after protease treatment. (**A**) Immunoblot of insoluble TDP-43 from cases with ALS, FTLD-TDP type A, type B, type C and Alzheimer's disease (AD) after trypsin treatment. Doublet bands at ~16 kDa (arrow) and some minor 23–24 kDa bands are detected in ALS and FTLD-TDP type B, whereas a single band at ~16 kDa and several bands at 23 and 24 kDa are detected in FTLD-TDP type A and type C. No such bands are detected in the Alzheimer's disease case. (**B**) Immunoblot of insoluble TDP-43 from cases with ALS, FTLD-TDP type A, type B, type C and Alzheimer's disease after chymotrypsin treatment. Multiple protease-resistant TDP-43 bands are detected at 16–25 kDa. Doublet bands at ~16 kD (arrow) are detected in ALS and FTLD-TDP type A and B, whereas a single band at ~16 kD (arrow) is detected in the case with FTLD-TDP type C. In FTLD-TDP type A, the lower band of the doublet at 16 kDa is more intense. No such bands are detected in the Alzheimer's disease case.

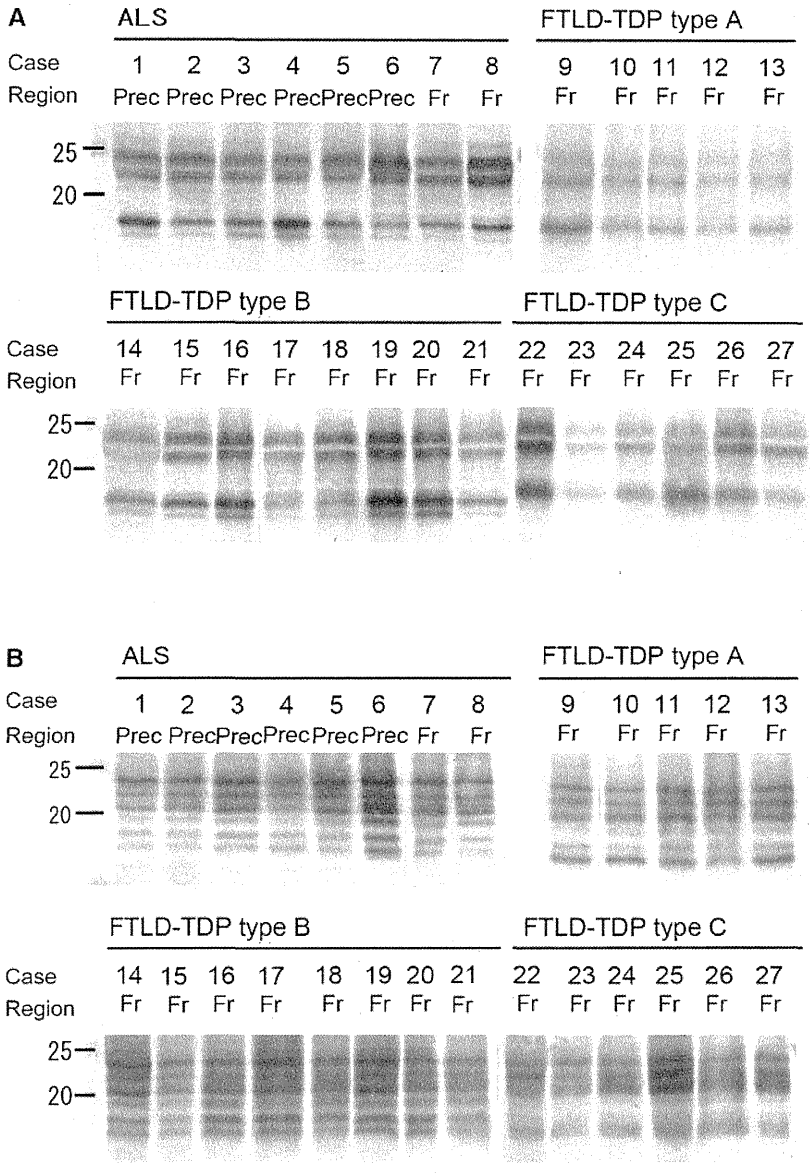

Figure 5 Comparison of the protease-resistant TDP-43 banding patterns in ALS and FTLD-TDP. Immunoblot analyses of trypsin-resistant (**A**) and chymotrypsin-resistant (**B**) fragments of TDP-43 from all cases examined. The banding patterns of ALS and FTLD-TDP type B cases are indistinguishable. Fr = frontal cortex; Prec = precentral gyrus.

In all cases examined, the trypsin-resistant banding patterns were clearly distinguishable between the disease subtypes in accordance with the three different types of banding pattern of TDP-43 C-terminal fragments, although it is difficult to distinguish the trypsin band pattern of type A from that of type C (Figs 5A, 6A and Supplementary Fig. 5). The chymotrypsin-resistant banding patterns were distinguishable and could be differentiated into three types (Figs 5B, 6B and Supplementary Fig. 6), also in accordance with the banding pattern of the TDP-43 C-terminal fragment. The banding patterns of ALS and FTLD-TDP type B were the same, whereas the banding pattern of FTLD-TDP type A was distinguishable from those of type C and type B (Figs 4 and 5). The combination analyses of trypsin and chymotrypsin-resistant banding patterns confirmed that TDP-43 proteinopathies can also be biochemically distinguishable into three types according to TDP-43 subtypes. These results strongly suggest that the different C-terminal banding patterns represent different conformations of TDP-43 aggregates and that the distinct types of TDP-43 are deposited in association with distinct pathological phenotypes of TDP-43 proteinopathies.

Immunoblot analysis using phosphorylation independent TDP-43 polyclonal and monoclonal antibodies detected some TDP-43 fragments in the ALS and FTLD-TDP cases after trypsin or chymotrypsin treatment, although no clear difference was observed in the banding patterns between ALS and other subtypes of FTLD-TDP (Supplementary Fig. 7). The distinctive

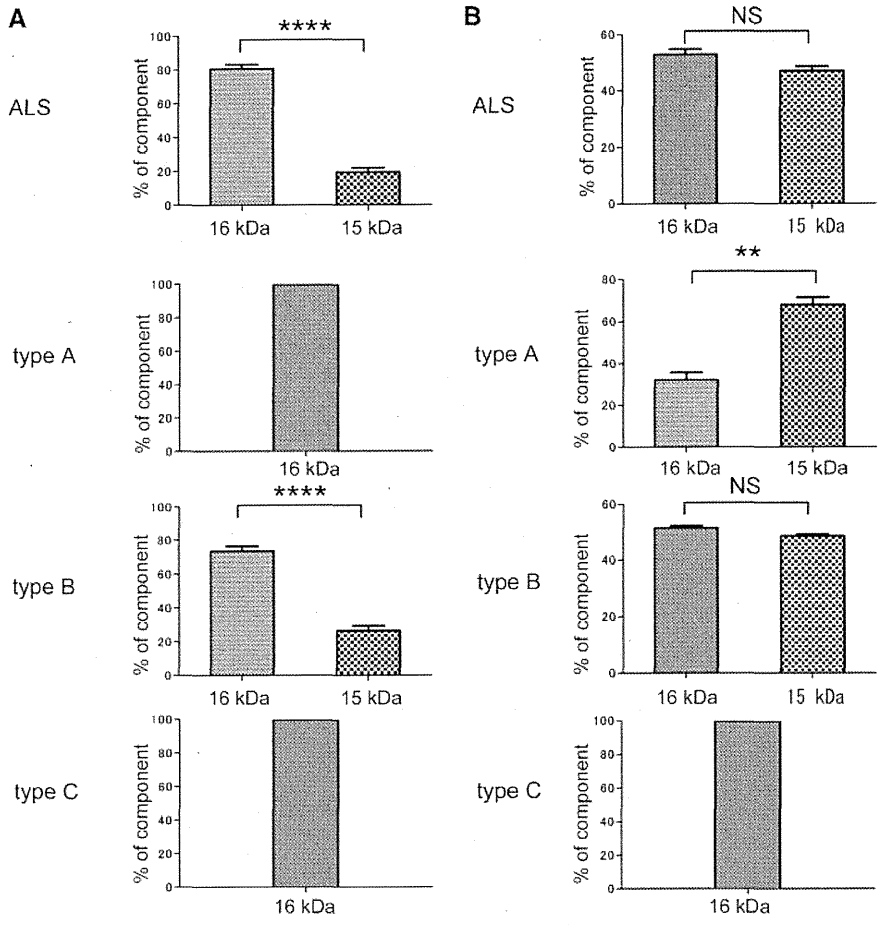

Figure 6 *Quantitative analysis of protease-resistant ~16 kDa band.* (**A**) *The intensity of trypsin-resistant ~16 kDa band of each case was* quantitated with ImageJ and statistically analysed. (**B**) The intensity of chymotrypsin-resistant ~16 kDa band of each case was quantitated with ImageJ and statistically analysed. Data indicate mean (SEM). $****P < 0.0001$, $**P < 0.01$, NS = not significant.

protease-resistant bands at ~16 kDa of ALS were not detected with both phosphorylation independent antibodies (Supplementary Fig. 8).

We also analysed the banding pattern of phosphorylated TDP-43 in another series of five sporadic cases with TDP-43 pathology (Alzheimer's disease, Alzheimer's disease/dementia with Lewy bodies and Alzheimer's disease/argyrophilic grain disease) (Supplementary Table 1). The banding pattern of the C-terminal fragments, and trypsin- or chymotrypsin-resistant fragments, in these were same as those of FTLD-TDP type A with *GRN* mutation (Supplementary Fig. 9).

Mass spectrometric analysis of protease-resistant bands of TDP-43 in ALS and FTLD-TDP type C

To further investigate the differences in the abnormal TDP-43 protein species at a molecular level, we analysed the ~16 kDa trypsin-resistant bands by mass spectrometry. Mass analysis of chymotrypsin digests of ~16 kDa trypsin-resistant fragments identified 4 peptides, amino acid residues 277–289, 290–299, 294–333 and 300–316, suggesting these peptides are derived from trypsin-resistant fragments 276–414 and 294–414. Mass spectrometric analysis of the single broad band from FTLD-TDP type C identified the peptides of amino acids 273–283, 277–289, 290–313 and 317–330, strongly suggesting that the trypsin-resistant fragments from FTLD-TDP type C are derived from peptides 273–414 and 276–414. These analyses clearly indicate that trypsin-resistant core regions of the abnormal TDP-43 accumulated in the brain are not necessarily the same between ALS and FTLD (Supplementary Fig. 10).

Discussion

In this study, we have shown that the banding patterns for TDP-43 C-terminal fragments in ALS and FTLD are distinguishable and classifiable into at least three types. This difference was consistently demonstrated in 27 cases, eight with ALS, five with FTLD-TDP type A, eight with FTLD-TDP type B and six with FTLD-TDP type C. These results strongly suggest that distinct